UNIVERSIDADE DE LISBOA

FACULDADE DE CIÊNCIAS

DEPARTAMENTO DE ENGENHARIA GEOGRÁFICA, GEOFÍSICA E ENERGIA

Linking meteorological fire danger and burnt area in Brazil under present and future climate conditions

Patrícia Santos Silva

Mestrado Integrado em Engenharia da Energia e do Ambiente

Dissertação orientada por:

Professor Doutor Carlos da Camara
Doutora Ana Bastos

2018

Acknowledgements

First and foremost, I would like to thank Professor Carlos da Camara and Ana Bastos, who have not only been the most wonderful and supportive supervisors but also great friends. Thank you for believing in me.

I would also like to thank my companions on this tough but amazing journey: Rúben, Adriana, Sofia, Matilde, Liliana, Catarina and Inês. A special and most heartfelt thank you to my dearest friend Daniela, whom I so admire and look up to.

To Ivo, my beloved boyfriend, who inspires me to do and be better, while being my shelter in the storm. Without your strength, love and care, my life would be much different and undoubtedly impoverished.

Lastly, but most certainly not least, to my family, without whom I could never be who I am or do what I've done. Carlos and Helena, with your hard work, courage and love, you've given me all the tools to succeed and I'll forever be thankful. Inês, your constant affection and support reminds me how lucky I am to have you by my side. Home will always be where you are.

This work was developed within the framework of the Brazilian Fire-Land-Atmosphere System (Br-FLAS) Project financed by the Portuguese and Brazilian science foundations, FCT and FAPESP (project references FAPESP/1389/2014 and 2014/20042-2).

Resumo

O fogo é uma das mais importantes perturbações ecológicas à escala local e global, afetando a distribuição e estrutura da vegetação, o ciclo do carbono e o clima. Os fogos emitem cerca de 2.2 PgC/ano (uma parcela significante comparativamente às emissões da indústria e combustíveis fósseis: 9.4 PgC/ano na última década) e têm impactos substanciais ao nível económico, social e de saúde. O fogo é comum no Brasil e na última década têm sido atingidos os maiores valores de área queimada desde que existem registos. No futuro, espera-se no Brasil um aumento moderado a elevado no potencial de fogo, uma transição para um clima mais seco e quente e uma maior probabilidade de ocorrência de eventos climáticos extremos. Fenómenos como secas e ondas de calor tornar-se-ão mais frequentes, estas últimas poderão vir a ocorrer a cada dois anos. Assim o estudo desta temática afigura-se essencial, de modo a fornecer às autoridades competentes a informação necessária ao planeamento e possível prevenção de fogos no futuro.

Neste estudo, usa-se um índice de risco de fogo desenvolvido para os biomas Brasileiros, o Meteorological Fire Danger Index (MFDI), desenvolvido pelo CPTEC/INPE, e um modelo regional de clima, o RCA4 do Rossby Centre (*regional downscaling* do EC-Earth para a América do Sul no âmbito do programa CORDEX), para avaliar a evolução do risco de fogo e área queimada em clima presente e futuro. O MFDI é utilizado operacionalmente no INPE para estimar valores diários de risco de fogo para a América Central e do Sul. O MFDI baseia-se no princípio de que quantos mais dias sem precipitação, maior o risco de fogo. O MFDI estima o quão propícia a vegetação está para ser queimada em determinado dia com base nas respectivas condições meteorológicas, nomeadamente temperatura máxima, humidade relativa mínima, precipitação acumulada e coberto vegetal. Para este último usou-se o mapa de vegetação do IGBP adaptado para o Brasil pelo INPE para 2005, e avaliaram-se os quatro *landcovers* predominantes: *Evergreen Broadleaf Forest* (*EBL*; inclui a Amazónia), *Closed Shrublands and Woody Savannas* and *Open Shrublands and Savannas* (*CSWS+OS*; inclui os biomas brasileiros cerrado e caatinga), *Croplands* (*C*) e *Grasslands* (*G*). Por último, é de notar que o MFDI é um indíce de perigosidade meteorológica, pelo que não considera a ignição nem a propagação do fogo.

O clima presente é avaliado recorrendo a três reanálises: ERA-Interim, MERRA-2 e NCEP-DOE Reanalysis II. Estas usam modelos para compilar de modo consistente observações de todo o globo (desde medidas no terreno a dados de satélite), constituindo assim o melhor conjunto de dados observacionais disponível à escala global. Adicionalmente, dados de área queimada são usados de forma a avaliar a capacidade do MFDI para reproduzir as condições atuais de fogo no Brasil. Para tal, recorreu-se ao produto AQM desenvolvido por Libonati *et al.* [2015] e calibrado para o Brasil usando dados do instrumento MODIS. Por outro lado, o clima futuro é avaliado usando o modelo regional de clima juntamente com os cenários de clima futuro RCP2.6, RCP4.5 e RCP8.5 do IPCC. Estes são denominados consoante o seu forçamento radiativo em 2100 (Wm^{-2}) e permitem simular possíveis trajectórias de emissões de gases com efeito de estufa, aerossóis, concentrações de gases na atmosfera e alterações no uso do solo.

O MFDI calculado por dados baseados em observações é comparado com informação de área queimada (BA), revelando-se capaz de replicar tendências de BA a nível inter e intra-anual. Observam-se diferenças entre valores de MFDI baseado nas reanálises: no geral, os dados do ERA-Interim conduzem aos maiores valores de MFDI enquanto que o NCEP conduz aos mais baixos (MERRA revela valores intermédios entre ambos). A reanálise ERA-Interim apresentam valores mais elevados de temperatura e mais baixos de humidade relativa, levando a um aumento do MFDI em todos os *landcovers* excepto

no *EBL* onde, devido a valores elevados de precipitação, o MFDI apresenta valores inferiores comparativamente às outras reanálises. Avaliando valores mensais totais de área queimada nos 12 anos de dados, verifica-se que os meses de maior BA são de Agosto a Outubro, pelo que estes foram considerados a época de fogos. A maior contribuição para a BA total é dada por *CSWS+OS* e a menor pelo *EBL*. Com estes resultados, simples modelos de regressão linear foram desenvolvidos para prever mudanças de área queimada usando o MFDI como preditor. Ao analisar a linearidade entre o MFDI calculado pelas reanálises e os dados de área queimada, escolheu-se o MFDI baseado nos dados ERA-Interim como preditor, dado que com este foram obtidos os maiores coeficientes de determinação em três dos quatro *landcovers* avaliados (representando 93% da área do Brasil) e ainda devido à sua maior resolução espacial. Os modelos foram ainda avaliados para diferentes períodos da época de fogos, onde se encontrou correlações mais elevadas em Agosto-Outubro para *EBL* e Setembro-Outubro para os restantes *landcovers*. Os modelos de área queimada resultantes são capazes de explicar pelo menos 50% da variância em todos os *landcovers* considerados (com resultados particularmente positivos para *CSWS+OS*, onde explicam 77% da variância).

Adicionalmente, o MFDI é calculado para condições de clima presente e futuro usando os resultados de simulações do RCA4. Em geral, o risco de fogo simulado apresenta curvas semelhantes às calculadas pelas reanálises, mantendo-se dentro dos valores observacionais na maior parte dos meses para todos os *landcovers*. Descobriram-se no entanto diferenças sistemáticas na temperatura em todos os *landcovers* e ainda diferenças significativas no campo da precipitação no *EBL*, que resultam em valores distintos de MFDI baseado em observações e simulações. É de salientar que tanto o MFDI baseado em simulações como o MFDI baseado em reanálises apresentam valores elevados no inverno austral, porém o pico do MFDI simulado dá-se em Setembro para o *CSWS+OS*, *C* e *G*, enquanto que o risco calculado com dados de reanálises ocorre um mês antes: desta forma, os dados do modelo resultam em maior risco de fogo no mês que arde mais. Para o futuro, o modelo calcula ainda um aumento de MFDI em todo o ano, especialmente na época de fogos, dado o aumento de temperatura e menor humidade relativa. Também é de notar um aumento de precipitação no verão austral para *CSWS+OS* e *C*.

Devido às discrepâncias encontradas, corrigiu-se a distribuição do MFDI (após testes de normalidade) de forma a aproximar o MFDI simulado ao calculado pelo ERA-Interim, resultado usado para prever futura área queimada usando os modelos de área queimada previamente desenvolvidos. De acordo com o aumento de MFDI estimado anteriormente, a BA tende também a aumentar ao longo do século: encontraram-se aumentos sistemáticos no valor médio comparativamente ao período histórico para todos os *landcovers* e cenários. Estes são especialmente notórios no RCP8.5, sendo o RCP2.6 o único cenário no qual o MFDI médio tem um menor valor no final do século comparativamente a meados do século (i.e. o risco de fogo diminui na segunda metade do século). *CSWS+OS* é o landcover que apresenta os maiores aumentos de média e desvio-padrão de BA quando comparado ao período histórico. Isto é de especial relevância considerando que este representa 76% da área queimada do Brasil.

Concluindo, alterações significativas nos parâmetros meteorológicos e um aumento do risco de fogo (e por consequinte, área queimada) são expectáveis para o Brasil nas próximas décadas. Estas alterações dependem em grande medida das trajectórias futuras de emissões de gases com efeito de estufa. É de notar, no entanto, as limitações deste trabalho: é usado um coberto vegetal estático, não tendo em conta as interacções entre o fogo e a vegetação; só é usado um modelo de clima regional, estando assim o estudo limitado à variabilidade interna e incertezas deste; e ainda que não é tido em conta a influência humana, nem a ignição e propagação do fogo.

Palavras chave: fogo, risco de fogo, área queimada, Brasil

Abstract

Fire is a key ecological disturbance, contributing to ecosystem structure, diversity and functioning. Fire emissions to the atmosphere amount to approximately 2.2 PgC/yr and fires have significant economic, social and health related impacts. Brazil is one of the most fire-affected areas in the globe and over the last decade the highest peaks in burned area have been observed since records began. Here, we employ a fire danger index tailored for Brazilian biomes, the MFDI, and outputs from a regional climate model, the RCA4 from the Rossby Centre, to assess present and future trends of fire danger and burned area. To that end, the MFDI as calculated by observation-based data was compared with a burned area (BA) dataset calibrated for Brazil (AQM, *Área Queimada*), with satisfactory results in both intra and inter-annual evaluations. Consequently, simple linear regression models were developed to predict changes in burned area using the MFDI as predictor, which were shown capable of explaining at least 50% of variance for all analysed landcovers. Conspicuous results were found for the Closed Shrublands and Woody Savannas + Open Shrublands and Savannas landcovers (*CSWS+OS*), which includes *cerrado* and *caatinga* biomes, where the burned area model explains 77% of variance. Using RCM results, MFDI based on simulated climate is evaluated for present and future climate conditions. Although simulation-based MFDI follows the overall trend of observation-based fire danger, a systematic underestimation of temperature was found for all biomes, accompanied with considerable differences in precipitation in Evergreen Broadleaf Forest landcover (which includes the Amazon rainforest). In the future, MFDI is expected to increase over the year especially in the fire season (August to October), consequence of higher temperatures and lower relative humidity throughout the year, and increased precipitation in austral summer, before the fire season, for *CSWS+OS* and Croplands. Lastly, model-based MFDI was approximated to observation-based distribution and used to estimate future BA using the burned area models previously developed. As expected from the increase in future MFDI, BA increases throughout the century: systematic increases in the mean BA from the historical period are found for all scenarios and all landcovers, which are especially pronounced in RCP8.5. RCP2.6 is the only scenario in which the mean by end of the century has a lower value than that of mid-century. In conclusion, although varying in magnitude, significant changes in meteorological parameters and higher fire danger (and consequently, burned area) are expected for Brazil in the coming decades.

Key words: fire, fire danger, burned area, Brazil

Contents

List of Figures

List of Tables

Acronyms

AQM Área Queimada

AVHRR Advanced Very High Resolution Radiometer

BA Burned Area

BAECV Burned Area Essential Climate Variable

CMIP5 Coupled Model Intercomparison Project Phase 5

CPTEC Centro de Previsão de Tempo e Estudos Climáticos

CWFIS Canadian Wildland Fire Information System

CORDEX COordinated Regional climate Downscaling EXperiment

CSR Cumulative Severity Rating

DOE Department of Energy

DSR Daily Severity Rating

ECMWF European Centre for Medium-Range Weather Forecasts

ENSO El Niño - Southern Oscillation

ESD Empirical-Statistical Downscaling

FFDI McArthur Forest Fire Danger Index

FIMMA Fire Identification, Mapping and Monitoring

FRP Fire Radiative Power

FWI Fire Weather Index

GCM Global Circulation Model

GHG Greenhouse Gases

GMAO Global Modeling and Assimilation Office

HIRLAM High Resolution Local Area Modelling

IBGE Instituto Brasileiro de Geografia e Estatística

IGBP International Geosphere-Biosphere Programme

IPCC Intergovernmental Panel on Climate Change

INPE Instituto Nacional de Pesquisas Espaciais

KBDI Keetch-Byram Drought Index

MERRA Modern-Era Retrospective analysis for Research and Applications

MFDI Meteorological Fire Danger Index

MODIS Moderate Resolution Imaging Spectroradiometer

NASA National Aeronautics and Space Administration

NCEP National Centers for Environmental Prediction

NFDRS National Fire-Danger Rating System

NOAA National Oceanic and Atmospheric Administration

RCM Regional Climate Model

RCP Representative Concentration Pathways

SRES Special Report on Emissions and Scenarios

UTC Coordinated Universal Time

1. Introduction

According to the Intergovernmental Panel on Climate Change (IPCC) the current concentrations of atmospheric CO_2, CH_4 and N_2O exceed any level registered in the past 800 000 years [IPCC, 2013]. During the past century, the observed average rate of increase of these gases surpassed any rate of change over the previous 20 000 years. Atmospheric CO_2 concentration is the main contributor to total radiative forcing, and its increase led to an energy imbalance of the Earth, estimated on the order of 0.5 to 1 Wm^{-2} over the past decade (Trenberth *et al.* [2014]; von Schuckmann *et al.* [2016]; Dieng *et al.* [2017]).

The IPCC [2013] deemed "extremely likely" that human influence has been the dominant cause of the consequent warming, observed since the mid-20^{th} century. A recent study has estimated that the human induced warming relative to the period 1850-79 is 1.01°C, essentially demonstrating that the observed warming since that period is mostly anthropogenic (the corresponding natural externally-driven change is -0.01 $\pm$ 0.03°C; Haustein *et al.* [2017]). The IPCC [2013] further disclosed that continued emissions of greenhouse gases will cause future warming and consequent changes in the climate system, and that these may persist for many centuries regardless of subsequent CO_2 reduction. Limiting these changes requires substantial and sustained reductions of greenhouse gas emissions. To evaluate how carbon dioxide concentrations and other influencing factors might impact future climate, the IPCC (AR5) defined four Representative Concentration Pathways (RCPs). These scenarios represent future emission trends, atmospheric concentration and land use change, among other factors, and are named according to their radiative forcing in 2100. Their results show that global temperature is expected to reach 1.5°C above pre-industrial levels in 2100 for all scenarios. An increase of 1.5°C is also the goal proposed in the Paris Agreement formulated in the COP21 meeting in Paris, in December 2015 [UNFCCC, 2017]. The meeting involved 196 parties (195 states plus the European Union) that agreed to undertake rapid reductions of CO_2 emissions in accordance with the best available science and in the context of sustainable development, while recognizing the need to support developing countries in their effective implementation of the Paris Agreement. According to Millar *et al.* [2017], limiting warming to 1.5°C is still physically achievable, however meaningful and quick action is required, and it strongly depends on how quickly pledges made in COP21 can be achieved.

Anthropogenic activity has been linked to global warming, to changes in the global water cycle, reductions in snow and ice and global mean sea level rise. Each of the last three decades has been successively warmer at the Earth's surface than any preceding decade since 1850. Over the last two decades, the Greenland and Antarctic ice sheets have been losing mass, and glaciers have continued to shrink worldwide. From 1901 to 2010 global mean sea level rose by 0.19 meters, and the rate of sea level rise since the mid-19^{th} century has been larger than the mean rate during the previous two millennia. Climate change can also lead to higher frequency and severity of extreme events and disturbances. This has become increasingly relevant in the past decades, as the world has seen more catastrophic events than ever before. The 2017 Atlantic hurricane season was marked by several extremely destructive hurricanes of categories 4 and 5, which caused widespread damage in the north-eastern Caribbean and Florida [NOAA, 2017]. Irma was the strongest storm on record to exist in the open Atlantic region, with winds of 295 km/h. Wildfires severely raged various regions of the globe in 2017: California saw its most costly fire season; British Columbia had its worst-ever wildfire season; and Portugal had its 2003 burned area record broken and the most fatal fire season on record [Nature Climate Change, 2017]. Some of

these events were exacerbated by severe droughts, whereas other regions of the globe were devastated by floods [Voiland, 2017].

Several studies have underlined the link between fire activity and climate change (e.g. Flannigan *et al.* [2013], Westerling *et al.* [2006] and Gillett *et al.* [2004]) and fire is arguably the most important disturbance agent in terrestrial ecosystems at a global scale, releasing every year significant amounts of carbon to the atmosphere (2.2 PgC/yr; van der Werf *et al.* [2017]). Estimates of global annual burned area range from 300 to 450 Mha, which is comparable to the size of India [Flannigan *et al.*, 2013]. This can have substantial impacts on vegetation structure and distribution, biogeochemical cycles, atmospheric chemistry and composition, as well as human health. Fire can disrupt ecological processes by reducing plant biomass and litter, thereby altering energy, nutrient and water fluxes between the soil, plants and atmosphere.

Wildfires are of particular importance in South America, as it is one of the regions most affected by fire along with the African and Australian continents [Bowman *et al.*, 2009]. Brazil covers a large area of South America, including most of the Amazon rainforest, and great efforts have been made to properly manage and study its frequent fire activity. Devastating fires have cut across Brazil in the last decade: according to the Brazilian National Institute for Space Research (INPE), 2017 was the most devastating year on record surpassing 2004, with 275 120 recorded fires; and September 2017 was the month with the highest fire activity since records began in 1998. In the previous decade several years surpassed the 230 000 recorded fires' mark, confirming the increased frequency of Brazilian wildfires (Figure 1.1).

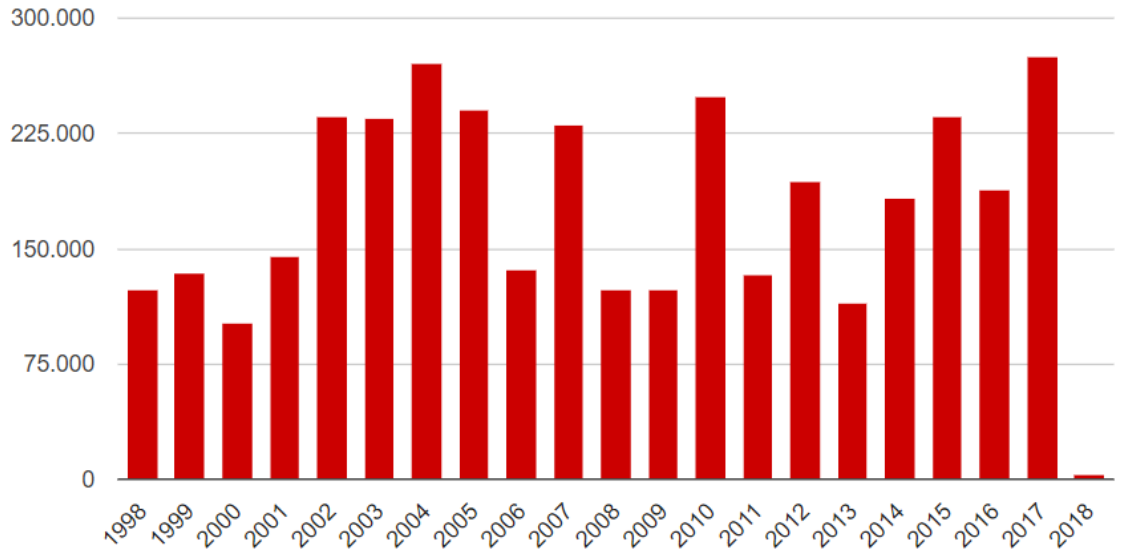

Figure 1.1: Inter-annual variability of fire activity from 1998 to present [INPE, 2017].

Although all Brazilian biomes are subjected to fire (to a greater or lesser degree), the Brazilian *cerrado* is particularly affected: according to Strassburg *et al.* [2017], it has lost 88 Mha (46%) of its native vegetation cover and only 19.8% remains undisturbed. *Cerrado* is the dominant vegetation of central Brazil, a savannah-like biome, covering approximately 25% of the country, and one of the most important global biodiversity hotspots [Myers *et al.*, 2000]. Although fire is a natural disturbance in savannahs, changes in fire regimes caused by human activity (either directly, through land use practices, or indirectly, affecting the climate) can have substantial impacts on these ecosystems. And *cerrado* is increasingly threatened, partly because of the absence of a consistent fire policy [Durigan and Ratter,

2016].

Furthermore, with increasing temperatures and drought, it is likely that Brazil will register an increase from moderate to high in wildfire potential, as well as a longer period of high fire potential and an increased likelihood of extreme weather events [Flannigan *et al.*, 2013]. However, most studies of future global fire patterns (e.g. Liu *et al.* [2010] and Brady *et al.* [2007]) are based on indices which are not tailored for the specific fire regimes under study, as they do not consider the region-specific biome characteristics and meteorology.

In this dissertation, a Brazilian fire danger index and outputs of a regional climate model are employed to assess present and future patterns of fire danger in the major Brazilian landcover types. The main goal is to assess fire danger and burned area changes under changing climate conditions over the 21^{st} century, to possibly provide a tool for scientists and policy makers to predict, and perhaps regulate, wildfire impact on climate, land productivity and management, and environmental protection. Special attention is paid to the *Closed Shrublands and Woody Savannas* and *Open Shrublands and Savannas* landcover type, given that it includes the Brazilian biomes *cerrado* and *caatinga*, and *Evergreen Broadleaf Forest*, which includes the Amazon rainforest, given their importance at the regional and global scale. In chapter 2, the relevant theoretical background is discussed, and in chapter 3 and 4 the datasets and methodologies used in this study are described. Chapter 5 holds the results, divided in four sub sections: an assessment is made in 5.1 of the capability of the fire danger index (as estimated using observation-based data) to accurately track the patterns and trends of burned area over Brazil under the climate conditions observed in recent decades; simple statistical models linking fire danger and burned area for each landcover are developed and evaluated in 5.2; the applicability of the fire danger index estimated from RCM outputs for the present is tested in subsection 5.3; and lastly, in 5.4. results from a statistical model of burned area using a meteorological index of fire danger as predictor are analysed for different climate change scenarios in the 21^{st} century. In chapter 6, the results are discussed in a comprehensive perspective, as well as possibilities for future studies.

2. Theoretical Background

2.1 Fire in the Earth System

Wildfire is often perceived as a natural hazard whose consequences are mainly negative, e.g. by destroying ecosystems and endangering populations. However, wildfire is a natural part of and plays a key regulating role in many environments. Fire clears the dead litter on forest floors which allows important nutrients to return to the soil, creating favourable conditions for animals and plants to develop. There are also tree species that rely on fire for reproduction: for example, seeds in pinecones are sealed with a resin that needs fire to melt and release the seeds. Hardesty *et al.* [2005] classified global vegetation in three categories: fire-dependent, fire-sensitive and fire-independent. Fire-dependent biomes are those that regularly burn constrained to the annual and seasonal climatological conditions, fuel accumulation, among other influencing factors. These ecosystems evolved with fire, which influences their structure and composition, and promotes regeneration. Fire-dependent biomes may have different fire regimes: grasslands and savannah regions are characterized by frequent, low-intensity surface fires, maintaining the open-structure characteristic to these biomes, whereas shrublands and some forest types may experience infrequent intense stand-replacing fires [Hardesty *et al.*, 2005].

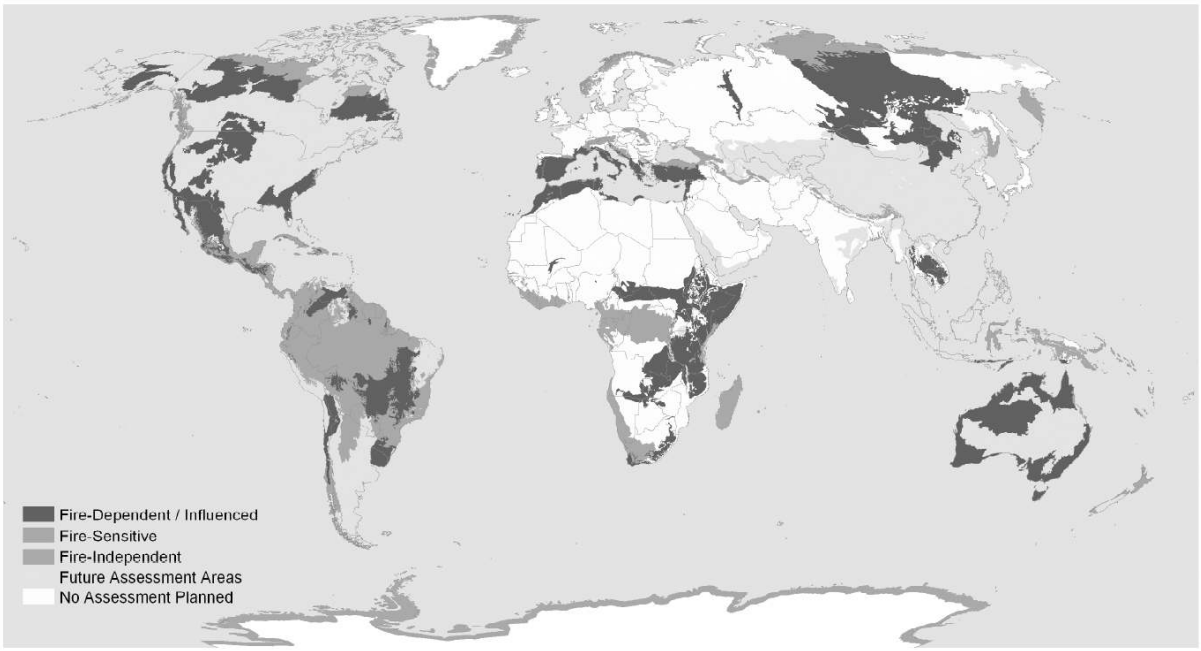

Figure 2.1: Fire-dependent, fire-sensitive and fire-independent regions [Hardesty *et al.*, 2005].

Regardless of how fire burns, fire-dependent ecosystems are characterized by resilient species and communities that have adaptations to enable them to thrive in fire-prone environments [Mutch, 1970]. On the other hand, in fire-sensitive ecosystems both fauna and flora are not prepared to sustain and recover from high fire activity. These ecosystems did not have until recently any major or frequent fire activity, thus are not able to positively respond or rebound after fire events. Frequent and intense fires can significantly change the structure, composition and functioning of these biomes, by selecting fire-adapted

species and favouring flammable species. The Amazon rainforest is one of such fire-sensitive ecosystems, where human-induced fires are altering its structure and composition. Finally, fire-independent biomes are those who see rare to no fire activity, such as the desert or tundra, mainly due to lack of fuel and ignition sources.

Almost half of global terrestrial area is fire dependent (about 46% according to Hardesty *et al.* [2005]) and, even though it does not capture as much attention, reduction of fire activity in fire-dependent regions can lead to significant disturbances in the community structure [Krawchuk *et al.*, 2009]. Similarly, altered fire regimes can profoundly change these biomes, as the above-mentioned species are not simply adapted to fire but rather to a set of environmental conditions that encompass the fire regime. Conversely, fire's beneficial effects in fire-prone regions can only occur if the fire does not burn for too long or with an intensity that causes the soil to be dry for an extended period. Only about 25% of the terrestrial world is considered to have intact fire regime characteristics (e.g., fire frequency, severity, extent and season, within their range of natural variability; Shlisky *et al.* [2008]), and direct or indirect changes in ecosystems seem to be inevitable.

A recent study found that the number of sites with no after-fire regrowth almost doubled after 2000, from 19 to 32%, comparing sites burned at the end of the 20^{th} century with those burned in the first decade of the 21^{st} century [Stevens-Rumann *et al.*, 2018]. The authors establish warmer and drier mean climate conditions as a key driver of these changes, and that there is a high likelihood that future wildfires facilitate shifts to lower density forests or non-forested areas under a warming climate. Although the study uses only a 23-year period, which is very short compared to the lifespan of a forest, its results are certainly relevant and worthy of reflection. In addition, Cochrane and Schulze [1999] reconstructed the historical fire activity near Tailândia (Pará, Brazil), and assessed that burned areas are more susceptible to repeated burns due to reduced tree cover and increased fuel loads. Both these results hint at the importance of fire in determining biome state. Staver *et al.* [2011] elaborates on fire-related biome transitions, showing how savannah and forests represent an alternative biome state. Fire can sustain savannah where climate favours forest by limiting tree cover and maintaining open canopies, further promoting favourable conditions for fire occurrence. As such, changed fire regimes associated with climate change, might lead to present-day forests transitioning to savannah regions; a process unlikely to be easily reversible. Large areas of South America and possibly Africa are identified as potentially at risk of changes in biome state. The Amazon rainforest in one of such regions with increased risk of biome transition, given the widespread deforestation, rising temperatures and the higher frequency of extreme drought events [Malhi *et al.*, 2009]. Furthermore, although it may not yet surpass the magnitude of natural variability, emerging evidence related to changing energy and water cycles, seems to indicate that the Amazon basin might be already in a biophysical transition to a disturbance-dominated regime [Davidson *et al.*, 2012].

Bond and Keeley [2005], used a dynamic global vegetation model to estimate the global biome distribution without fire, where the only controlling parameter would be climate (Figure 2.2). Their results show that closed forests, which currently cover a quarter of the globe, would more than double in extent when considering only climate constraints. All the higher rainfall sites showed a tendency to form forest following suppression of fire, in which biomes such as grasslands and savannah, namely those in more humid regions (such as the Brazilian *cerrado*), present the most pronounced results. These are also the biomes with the highest amount of fire events, which highlights the relevance of disturbance agents in shaping global vegetation distribution.

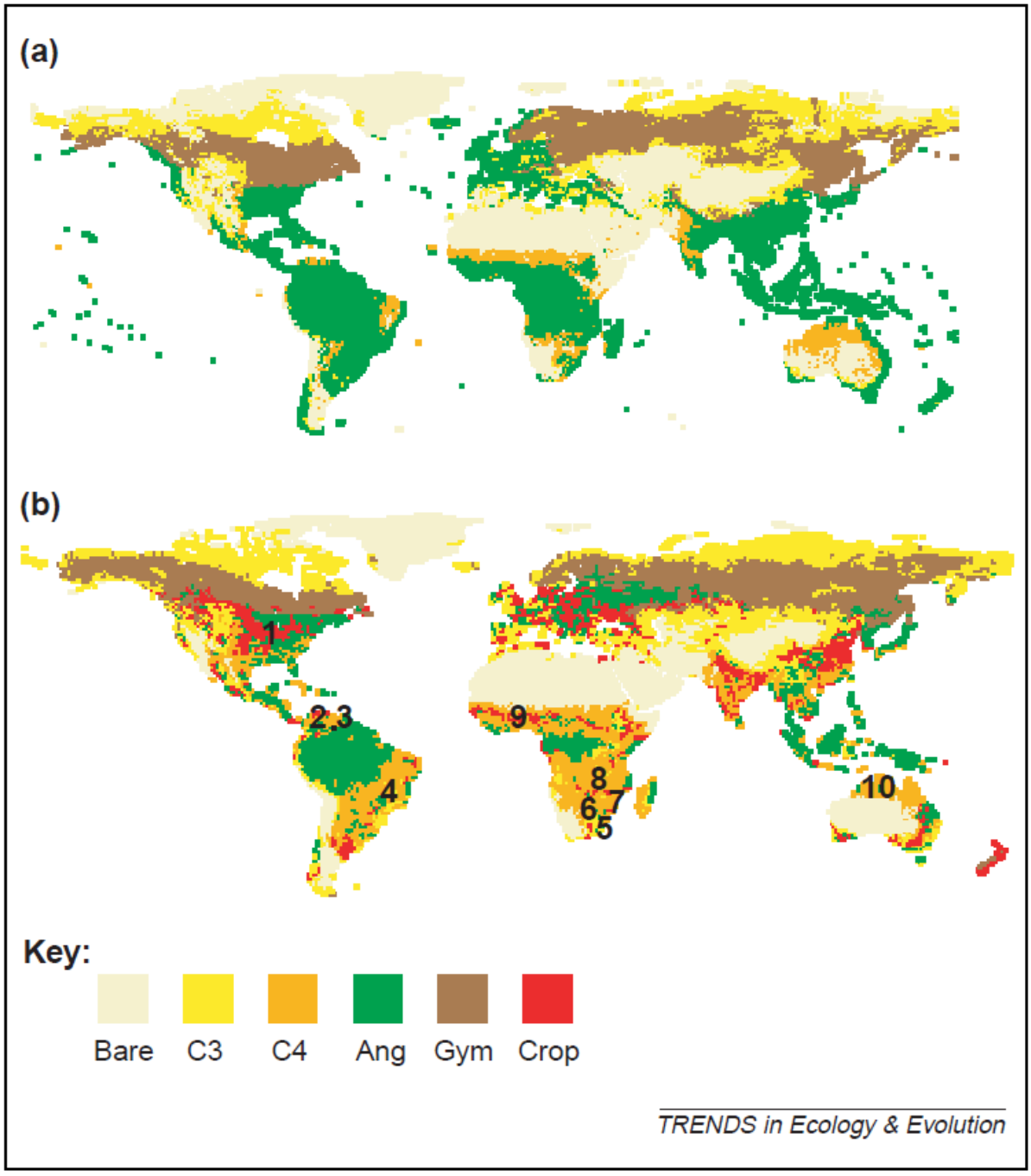

Figure 2.2: Global biome distribution at: (a) climate potential and (b) actual vegetation. Biomes types, represented by the cover of the dominant plant functional type: C3 - grasses or shrubs; C4 - grasses or shrubs; Ang - angiosperm trees; Gym - gymnosperm trees. The numbers indicate sites where fire has been excluded for several decades [Bond and Keeley, 2005].

Disturbances may alter the state and trajectory of an ecosystem, being key drivers of spatial and temporal heterogeneity [Turner, 2010]. In Yellowstone, for example, the 1988 fires created a complex spatial mosaic of patches that varied in size, shape, and severity [Turner *et al.*, 1994]. A recent study using 12 years of satellite data, estimates that degradation and disturbance of ecosystems represent 70%, 81% and 46% of carbon losses in tropical America, Africa and Asia, respectively. In Baccini *et al.* [2017], forest degradation and disturbance is defined as "losses in carbon density in a forest that remains forest" which includes processes such as drought or wildfires. They further add that ending degradation and disturbance could reduce emissions by at least 862 TgC/yr, possibly paving a path for a low-emission

future. These results are supported by similar findings estimating that most fire-related carbon emissions in South America are due to tropical deforestation and degradation and to savannah, grasslands and shrubland fires [van der Werf *et al.*, 2017]. In the period of 1997 to 2016, the same study found that, globally, fires emit approximately 2.2 PgC/yr to the atmosphere. These emissions represent a significant contribution when compared to those of fossil fuels and industry, which have increased from 3.1 $\pm$ 0.2 PgC/yr in the 1960s to an average of 9.4 $\pm$ 0.5 PgC/yr in the past decade (2007-2016) [Le Quéré *et al.*, 2017]. To achieve the goals established by the Paris Agreement for 2100, it is important to include and recognize fire as a driver of biogeochemical cycles and ecosystem processes. Increased fire and limited regeneration can significantly contribute to increased concentrations of carbon in the atmosphere, as not only fire themselves release carbon as they also decimate the forests which would consume it. Furthermore, when associated with carbon stock deposits, fires expedite the release of more carbon to the atmosphere, as happened in the 1997 massive fires in Indonesia that resulted in vast deposits of peat burning. Most of the carbon released in these fires is from the slow accumulation of C-stocks rather than the burning of forest trees [Schimel and Baker, 2002]. The major fire activity in this event released an equivalent quantity to the global carbon uptake by the terrestrial biosphere in a typical year [Page *et al.*, 2002].

Furthermore, pyrogenic carbon (charcoal) is hypothesized to play an important role in the carbon cycle given its high resistance to decomposition, and although it was found that fire severity does not influence the amount of PyC created, it influences its distribution: PyC in the forest floor becomes susceptible to erosion, emitting carbon to the atmosphere at an increased rate than those in the trees. High severity fires such as the 1997 event can also lead to an increase in pyrogenic carbon (PyC) in aboveground areas whereas low-to-moderate severity fires increase PyC in the forest floor [Maestrini *et al.*, 2017].

2.1.1 Pyrogeography

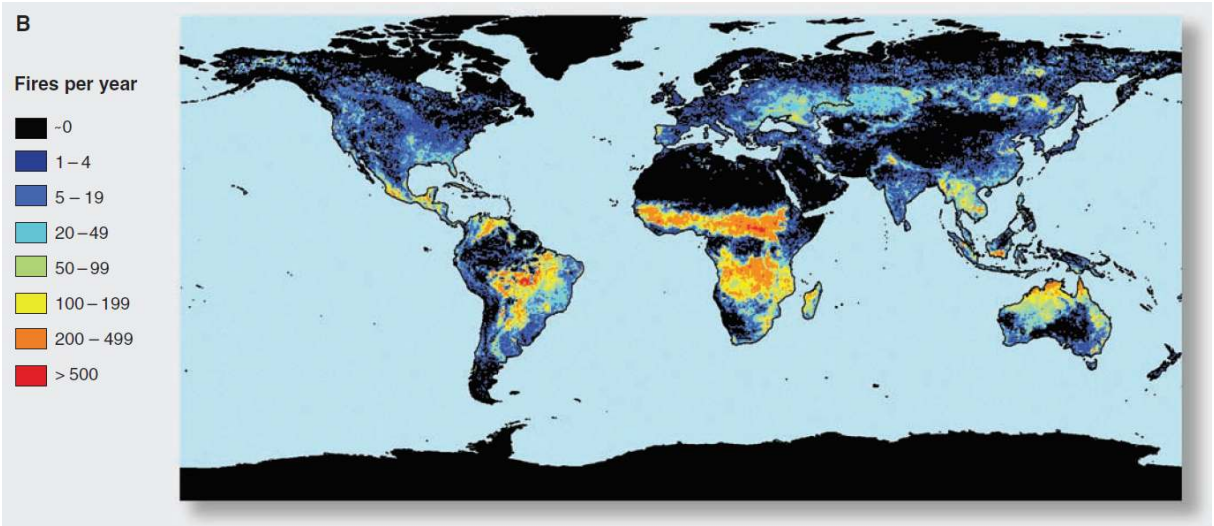

Figure 2.3: Current global pyrogeography illustrated by annual average number of fires, using satellite data [Bowman *et al.*, 2009].

As a major component of the Earth System, the study of fire and its drivers, impacts and resulting feedbacks with climate and ecosystems, becomes essential. Emerging satellite-derived data has provided global datasets to describe the distribution, variability and seasonality of burning. The study of the

distribution of fire that attempts to quantify observed variability in fire activity as a function of the complex interplay of environmental factors, is called pyrogeography [Moritz *et al.*, 2010]. It is worth noting that pyrogeography only regards the distribution of fire, and that other fire regime elements such as seasonality, intensity, burned area and frequency, also need to be taken into account when evaluating fire activity [Turner, 2010]. Nevertheless, pyrogeography allows to explore the global spatial distribution of fires and attempt to quantify their causes and effects, examining the link between environmental change, vegetation and fire.

Similarly to how biomes are differentiated (using vegetation traits), Archibald *et al.* [2013] identified regions with similar fire characteristics and defined five global units of fire using remotely sensed imagery, based on five fire regimes characteristics: fire return interval, maximum fire intensity, length of the fire season, maximum fire size and mean annual burned area. The identified pyromes were: larger and intense fires (frequent-intense-large, FIL); smaller and less intense fires (frequent-cool-small, FCS); infrequent, high intensity and larger fires (rare-intense-large, RIL); infrequent, lower intensity and smaller fires (rare-cool-small, RCS); and lastly, intermediate fire return times and small fires (intermediate-cool-small, ICS) (Figure 2.4). Correlation with biomes was investigated, in which they found that biomes such as boreal forests or tropical grasslands are dominated by a specific pyrome type: 93% of boreal forests fall into the RIL and RCS pyromes; whereas FIL and FCS dominate in tropical grasslands. Moreover, all biomes contain a substantial portion ($>$ 20%) of the ICS pyrome. They further explored the link between pyromes and meteorological parameters (namely, mean annual temperature and mean annual precipitation) and found that frequently burning pyromes dominate in arid ecosystems and are also associated with strong rainfall seasonality, which provides frequent opportunities for fire by promoting biomass (fuel) growth in the wet season and fuel drying subsequently. They also suggest that human activity is disrupting the fire system and plays an equal role to climate in determining current pyromes.

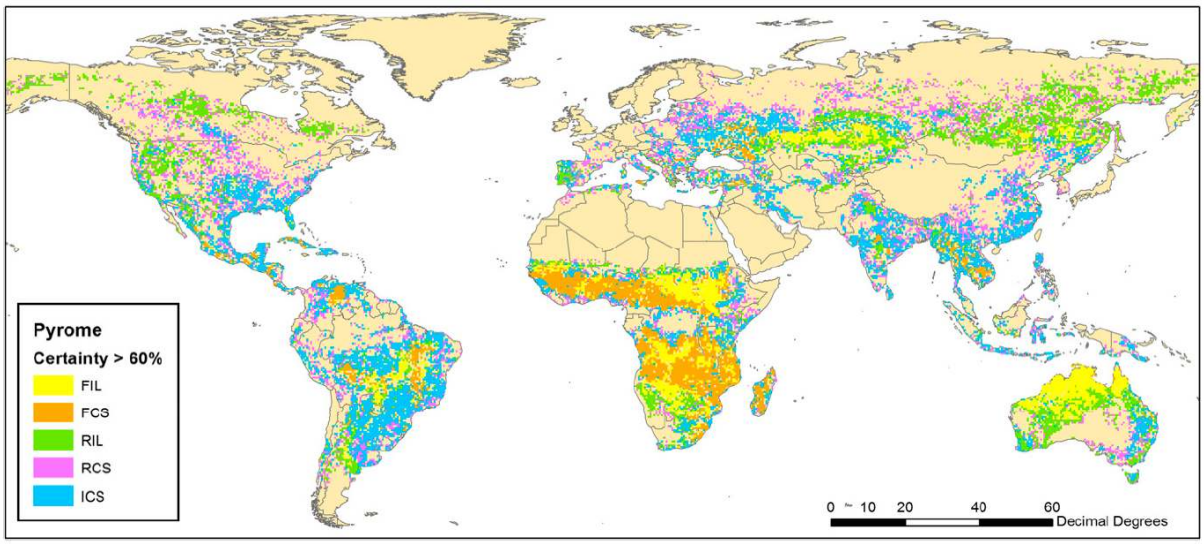

Figure 2.4: Spatial distribution of pyromes [Archibald *et al.*, 2013]. Australia is mainly characterized by the FIL pyrome (yellow), whereas Africa presents a large area in both the FIL and FCS pyrome (orange). South America seems to be dominated by ICS pyrome (blue), which occurs mainly in regions of deforestation and agriculture, and a significant part of central South America has FIL and FCS pyromes which seems to be in accordance with the *cerrado* biome.

It is commonly accepted that fire behaviour has a strong link to both land-use practices and meteorological conditions (Aldersley *et al.* [2011]; Hoffmann *et al.* [2012]). The latter controls the amount of fuel available for burning, its flammability (defined as "the capacity for vegetation to be ignited at flash point" by Phillips et al., 1974) and combustibility ("the capacity to sustain fire and to remain alight"), given that

vegetation growth and its moisture content rely on meteorological factors such as temperature, precipitation and relative humidity. Temperature holds a threefold role in fire dynamics [Flannigan *et al.*, 2013]: with increasing temperature, evapotranspiration increases as well and, as the ability for the atmosphere to hold moisture increases rapidly with higher temperatures, fuel moisture will decrease (unless there are significant increases in precipitation); with warmer temperatures there may be more lightning activity, which leads to increased natural ignitions; lastly, higher temperatures may lead to a lengthening of the fire season. Libonati *et al.* [2015] further demonstrates that the inter-annual variability of burned area in the Brazilian *cerrado* is closely related to the inter-annual variability of precipitation, where the years with largest annual amounts of burned area are those with the lowest amounts of annual precipitation. In the future, Brazil is expected to become drier (Marengo *et al.* [2012]; Duffy *et al.* [2015]; Guimberteau *et al.* [2013]) and warmer [Moritz *et al.*, 2012], affecting ecosystems and promoting conditions for fire activity (Silva *et al.* [2016]; Le Page *et al.* [2017]).

2.1.2 Fire, meteorology and human activity

Beckage *et al.* [2005], suggests that climate-fire relationships could provide a general basis for understanding the natural seasonality and frequency of fire, based on case studies from the United States of America. They hypothesize that these relationships allow to infer historical fire regimes and their variability using data on past climate, such as El Niño-Southern Oscillation (ENSO) reconstructions over the past thousands of years.

Meteorology also drives primary productivity and biomass decomposition, which are closely related to fire activity. Krawchuk *et al.* [2009] developed a statistical modelling framework capable of successfully reproducing current-day global fire patterns, using an ensemble of multivariate statistical generalized additive models. Their results reinforce that the existence of fuel is necessary for wildfires to occur, in which areas with low levels of vegetative resources to burn had a low probability of fire. However, they also found that the influence of vegetation is limited by environmental constraints on fire activity. Central Amazon for example is relatively fire-free, even though it is one of the most biomass-rich areas in the world: although they have available vegetative resources to burn, areas such as this rarely experience environmental conditions that promote biomass burning. Similarly, Pausas and Ribeiro [2013] introduce the "intermediate fire-productivity" conceptual model, where fire activity is highest in environments with intermediate aridity/productivity, such as tropical savannah. On the other hand, fire activity is low in unproductive, typically arid environments, given the absence of biomass; and in mesic, productive environments (such as rainforests) because fuel is rarely dry enough to burn. They further elaborate on the non-linear relationship between droughts, fuel and fire regimes. Droughts can drive fire activity in humid and productive regions where fuel is highly available, whereas in unproductive and arid environments fire activity is fuel-limited. Increased drought frequency might induce more fires, whereas in unproductive ecosystems more droughts could possibly reduce fires as it would limit plant growth and fuel loads. As such, the impacts of such extreme events in the context of global change can vary significantly depending on the ecosystem. Nevertheless, extreme events such as droughts or heatwaves can potentially aggravate fire events by increasing the probability of high severity occurrence. In South America such events are particularly influenced by variations in climate conditions arising from atmosphere/ocean interactions such as ENSO [van der Werf *et al.*, 2004]. The Amazon is particularly sensitive to ENSO-related droughts, increasing its probability of drought-induced and high severity fires [Schimel and Baker, 2002]. In the last two decades, large areas of the Amazon basin experienced the most four severe droughts ever recorded, namely the 1997/1998, 2005, 2010 and 2015 events, with a significant

increase in the coverage area and intensity [Panisset *et al.*, 2018] . At the same time, heatwaves have been increasing in South America and particularly in Brazil (Perkins *et al.* [2012]; Rusticucci [2012]; Geirinhas *et al.* [2017]) and could, by the end of the century, be as frequent as every 2 years [Russo *et al.*, 2014].

Nevertheless, as mentioned before, fire is not only constrained and influenced by meteorological parameters. In fact, fire's behaviour has a strong linkage to human activity with anthropogenic factors explaining e.g. most of the variance in fire size [Hantson *et al.*, 2015]. In South America, human factors might even outweigh climatic drivers [Aldersley *et al.*, 2011]. Activities such as logging increase flammability of the forest, by reducing forest leaf canopy coverage by 14-50%, allowing sunlight to penetrate the forest floor and drying the organic debris left by the activity, and thus increasing vulnerability to future fires [Brando *et al.*, 2014]. As such, given the importance of human activity, it is essential to communicate fire vernacular in a consistent and coherent way. Hardy [2005] discusses the importance of having a clear and concise terminology, and resorts to several studies to define various terms in the fire vernacular. As opposed to "fire risk" that addresses values or damages, "fire danger" refers only to the probability of fire ignition, with both anthropogenic and natural causes. The term "hazard" must only be used to express the state of the fuel complex and is independent of weather or the environment in which the fuel is found. "Severity" is not a concise term, as it concerns the characterization of the effects of fire on wildland systems not the fire itself. Also, expressions such as "catastrophic" are not used in the fire community, as it derives from expressions of social, cultural and economic value. On the other hand, Williams [1977] defines "fire spread" as a meaningful concept only under situations in which both burning and non-burning combustibles are identified, as it can occur only if there is some type of communication between the burning region and the non-burning fuel. This dissertation focuses on the predisposition of vegetation to be burnt and as such, following Hardy [2005], the term "fire danger" will be used to refer to probability of fire ignition as constrained by vegetation and climate.

2.2 Evaluating climate

Given the importance of studying fire as a key process in the Earth System [Bowman *et al.*, 2009], studies often rely on climate modelling. Global Circulation Models (GCMs) provide a quantitative description of the physical processes in the atmosphere, ocean and land surface and are crucial to the understanding of climate. Although they have been highly improved in recent years, the low horizontal resolution of GCMs (in the order of lat/lon degrees) does not allow an accurate representation of important regional processes and forcings (including topography and other land-surface characteristics). This takes special importance when studying extreme events, which are highly dependent on regional conditions and which GCMs resolution dissolves, especially when analysing higher-order climate statistics [Giorgi *et al.*, 2009].

To tackle these limitations, several attempts have been made to perform climate simulations at finer grids. These downscaling methods are divided into two categories [Giorgi *et al.*, 2009]: empirical-statistical downscaling (ESD) and dynamical downscaling. The former uses statistical relations between global predictors and regional variables of interest, assuming that these statistical formulas are valid in the past, present and will still be valid in the future. Dynamical downscaling, on the other hand, uses numerical representations of the physical processes that create the climate system to estimate the different meteorological parameters, assuming such process remain the same. These are also called Regional Climate Models (RCMs) and they use the outputs of GCMs as boundary conditions (meteorological parameters, e.g. wind components and temperature, and surface parameters, e.g. sea surface temperature) [Giorgi, 2006].

The COordinated Regional climate Downscaling EXperiment (CORDEX) is an initiative sponsored by the World Climate Research Programme aiming to provide a framework for the evaluation and improvement of regional downscaling [Giorgi *et al.*, 2009]. Although there have been several regional climate model intercomparison projects implemented throughout the years, their lack of common frameworks and protocols has proven to be a disadvantage, neither allowing the characterization of uncertainties nor the transfer of knowledge between different domains. The CORDEX project attempts to address this issue, providing a common framework to allow coordinated sets of regional downscaling experiments worldwide. This common framework includes the division of the world into 14 domains (Figure 2.5), covering essentially all land areas of the globe, allowing the working groups to perform their experiments within the same boundaries; and using a finer grid resolution. The climate projection framework aims to produce a large ensemble of future projections based on various models (both RCMs and GCMs) for the 21^{st} century using IPCC's scenarios, the Representative Concentration Pathways (RCPs) [IPCC, 2013].

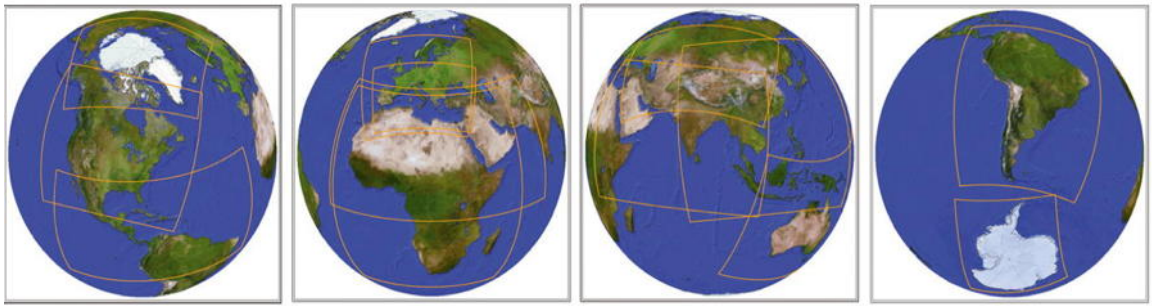

Figure 2.5: The common domains used in the CORDEX framework. It should be noted that these domains represent interior analysis domains, not including the lateral relaxation zone in RCMs [JPL, n.d.].

The RCPs defined by the IPCC replace the previous SRES scenarios (Special Report on Emissions and Scenarios) and are named according to the expected value of additional radiative forcing in 2100 relative to the pre-industrial period, expressed in Wm^{-2}, representing the additional energy taken up by the Earth system due to the enhanced greenhouse effect compared to the non-perturbed energy budget. Total radiative forcing is determined by both positive forcing from greenhouse gases and negative forcing from aerosols. These RCPs represent different pathways of GHG emissions, atmospheric concentrations, aerosols and land use, into the future (Figure 2.6). Contrary to the SRES scenarios, parameters such as population growth, economic development or technology are not static, which allows to explore different socio-economic schemes leading to the same level of radiative forcing.

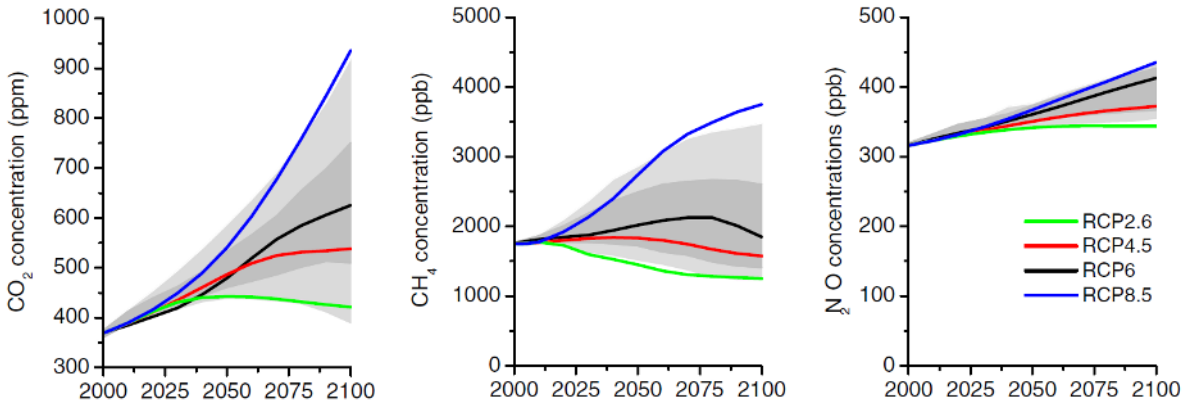

Figure 2.6: Trends in concentrations of greenhouse gases [van Vuuren *et al.*, 2011].

Four scenarios were defined by the IPCC to explore four levels of radiative forcing: RCP2.6, RCP4.5, RCP6 and RCP8.5 (Figure 2.7). The first scenario does not compare to any former SRES scenarios (while the other three do) and contemplates the most ambitious greenhouse emissions reductions. It was developed by PBL Netherlands Environmental Assessment Agency, and radiative forcing reaches its maximum value at 3.1 Wm^{-2} before it returns to 2.6 Wm^{-2} by 2100. Both RCPs 4.5 and 6 correspond to intermediate emissions scenarios, developed by the Pacific Northwest National Laboratorys Joint Global Change Research Institute in the United States of America and the National Institute for Environmental Studies in Japan, respectively. The former is comparable with SRES scenario B1 and the latter with SRES scenario B2. Finally, RCP8.5 was developed by the International Institute for Applied Systems Analysis in Austria and is consistent with a future with no policy changes to reduce emissions. RCP8.5 could be considered the business-as-usual scenario (although such denomination is not advisable) and is comparable with SRES scenario A1 F1.

Scenario Component	RCP2.6	RCP4.5	RCP6	RCP8.5
Greenhouse gas emissions	Very low	Medium-low mitigation Very low baseline	Medium baseline; high mitigation	High baseline
Agricultural area	Medium for cropland and pasture	Very low for both cropland and pasture	Medium for cropland but very low for pasture (total low)	Medium for both cropland and pasture
Air pollution	Medium-Low	Medium	Medium	Medium-high

Figure 2.7: Table with the main characteristics and differences between RCP scenarios [van Vuuren *et al.*, 2011].

Even though state-of-the-art GCMs and RCMs simulations for the RCP scenarios are the best estimates available of future climate trajectories, it is crucial to understand that these experiments present several sources of uncertainty [Evans, 2011]:

1. The future anthropogenic emissions are not known nor can they be accurately estimated as they heavily rely on future policy and human activities;

2. The model configuration of the different GCMs and RCMs also provides another source of uncertainty, as different models have different modelling approaches and can provide plausible scenarios

for the future as long as they are successful in replicating present climate conditions;

3. The internal (natural) variability of climate in the GCMs and RCMs simulations is also an issue, namely for slow developing components such as oceans and vegetation;

4. There are biases and systematic errors associated with the GCMs (which propagate on the RCM and ESD model runs) and on the ESD/RCM models themselves. Natural variability also increases at finer scales, which complicates the detection of anthropogenic signals.

As such, caution must be used when analysing climate projections from GCMs and RCMs. Our knowledge of Earth system processes is limited and imperfect, and care must be taken to extract information from these models with confidence. Although quantifying uncertainties from models is an area of research in need of much more attention than it gets [Gutowski *et al.*, 2016], these errors should not be taken as evidence that their results are completely amiss [Brown and Caldeira, 2017]. However, the lack of understanding of physical processes becomes more significant as the scale of interest becomes finer. The CORDEX experiment can provide some enlightenment on some of the above-mentioned concerns by: (1) using different climate change scenarios to encompass several possible futures; (2) analysing the internal variability of RCMs by creating several experiments with the same RCM and scenario but changing its initial conditions; (3) evaluating model configuration of GCM models, using different GCMs with the same RCM and scenarios, and evaluating model configuration of RCM models by experimenting different RCMs with the same GCM boundary conditions and scenarios. In this dissertation, we only tackle concerns (1) and (2), as the remaining would require the use of several RCMs and GCMs.

In the scope of the CORDEX project, RCMs are also evaluated in a set of historical experiments using reanalysis products (namely, the ERA-Interim reanalysis). The resulting data is then compared to observational datasets to ensure a meticulous analysis of the models' behaviour. Atmospheric reanalyses provide a numerical description of the recent climate, based on an unchanging data assimilation scheme and a model processing the available observations [ECMWF, n.d.]. Not all reanalysis data is constrained by observations: some estimates, namely those related to the hydrological cycle, such as precipitation and surface evapotranspiration (for which global observations simply do not exist), are obtained by running numerical weather prediction forecast models [Nigam and Ruiz-Barradas, 2006]. The input observations are taken from multiple sources ranging from early in-situ surface observations to modern high-resolution satellite datasets. These must be collected and prepared to enter the data assimilation system and ensure spatial and temporal consistency in the datasets [ECMWF, n.d.]. This allows a better understanding of climate processes, by incorporating an extensive number of observational data that no individual could collect and analyse separately. It is worth noting that replacement or changes to instruments and data retrieval methods may induce errors, and the changing observation methods can produce variability and spurious trends which are troublesome to understand and quantify [Dee *et al.*, 2016]. Furthermore, all estimated variables have their limitations: if it is constrained by observations; directly or indirectly observed; how it changes in time; and how accurately the model can predict a given variable.

2.3 Evaluating fire

Several approaches have been developed to evaluate present and future fire trends, and capture climate-vegetation-fire feedbacks. Some studies incorporated a process-based fire module into dynamic global vegetation models, which simulate climate-based processes controlling fuel availability (e.g. Thonicke *et al.* [2010] and Prentice *et al.* [2011]). Fire can also be estimated using statistical models of fire activity,

based on empirical relationships with key environmental variables (e.g. Chen *et al.* [2011], Moritz *et al.* [2012] and Pausas and Ribeiro [2013]).

2.3.1 Present fire conditions and burned area

Present fire is usually evaluated using burned area datasets, obtained with satellite remote-sensing data. These allow the detection and monitoring of active fires at local and global scales and provide consistent and extensive burned area datasets covering multiple years.

The Landsat program has launched a series of satellites, providing repetitive acquisition of high resolution multispectral data of the globe, with 30 m spatial resolution and 185 km swath. Being the longest record of the Earth's continental surfaces as seen from space, Landsat's orbit swaths are wide enough for global coverage every season of the year and its images detailed enough to characterize human-scale processes (e.g. urban growth, agricultural irrigation and deforestation). The Burned Area Essential Climate Variable (BAECV) algorithm was developed using Landsat imagery, to automatically identify burned areas regardless of ecosystem type and without ancillary data to direct its search [USGS, 2017]. BAECV uses a gradient boosted regression model and a thresholding process [Hastie *et al.*, 2009] to identify the date of the Landsat scene with the highest burn probability. Similar to the BAEVC, the Fire Identification, Mapping and Monitoring (FIMMA) product is an threshold algorithm, used to detect fires using multichannel measurements from the Advanced Very High Resolution Radiometer (AVHRR) data from National Oceanic and Atmospheric Administration (NOAA) polar-orbiting satellites [Li *et al.*, 2000]. The AVHRR is a radiation-detection imager used for remotely determining cloud cover and the surface temperature, with 1 km resolution. Nevertheless, the FIMMA is only accurate over forested regions and may miss fires over urban and agricultural areas.

The Moderate Resolution Imaging Spectroradiometer (MODIS) outputs are also widely used to analyse the global distribution of biomass burning. MODIS is a key instrument aboard the National Aeronautics and Space Administrations (NASA) Terra and Aqua satellites, which cover the entire Earth's surface every 1 to 2 days, acquiring data in 36 spectral bands ranging in wavelength from 0.4 μm to 14.4 μm [Giglio *et al.*, 2009]. Their data are used to create various global datasets: the Burned Area product, which uses MODIS to locate the occurrence of rapid changes in daily surface reflectance time series data and approximate date of burning at 500 m resolution; and the Active Fire product, detecting fires in 1 km pixels that are burning at the time of overpass under relatively cloud-free conditions using a contextual algorithm. Combining both Burned Area and Active Fire products, comprehensive datasets of BA are developed: the MCD64 burned-area mapping approach employs 500 m MODIS imagery coupled with 1 km MODIS active fire observations. The combined use of active-fire and reflectance data enables the algorithm to adapt regionally over a wide range of pre and post-burn conditions and across multiple ecosystems [Giglio *et al.*, 2016].

Specially tailored for Brazil, the *Área Queimada* (AQM) product uses a burn-sensitive vegetation index based on top-of-the-atmosphere values of middle infrared radiance and near infrared reflectance, acquired from the MODIS instruments [Libonati *et al.*, 2011]. It also relies on active fire observations obtained using fire detection algorithms produced by INPE, which are being fed continuous data from several satellite instruments. When compared to MODIS burnt area products (MCD45A1 and MCD64A1) for Brazil, AQM shows increased performance and better agreement with high-resolution Landsat data, with noticeable results for the *cerrado* region where it can more accurately identify burned areas with a lower number of omission errors [Libonati *et al.*, 2015]. The AQM dataset has also been successfully used to study the Amazonian forest-savannah [Wuyts *et al.*, 2017].

Moreover, the MODIS Burned Area datasets can also be combined with other remote sensing products to further improve fire assessment: the Global Fire Emissions Database combines MODIS BA data with active fire data from the Tropical Rainfall Measuring Mission Visible and Infrared Scanner, and the Along-Track Scanning Radiometer family of sensors, to create global monthly burned area datasets at 0.25°spatial resolution from mid-1995 through the present Giglio *et al.* [2013]. This BA component is used to estimate fire emissions, in an attempt to understand the role of biomass burning in the global carbon cycle and within the Earth system.

Dwyer *et al.* [2000] used data from AVHRR, over 21 months of global daily satellite data at 1 km grid resolution, to determine the positions of active vegetation fires. They found that fires occur throughout the year, however there is a strong spatial and temporal variability; although most of fire events are located in the tropics, a significant amount of fire activity was also present in temperate and boreal regions. Giglio *et al.* [2006] used MODIS at 0.5°spatial resolution to analyse the global distribution of biomass burning, from November 2000 to October 2005. They further introduce the remotely sensed mean fire radiative power (FRP) to indirectly calculate the total energy released during combustion, and thus the mass of fuel consumed given the heat of combustion for that fuel. Using FRP they have found that, at the global scale, July, August and September are the peak months of fire occurrence, both for the northern and southern hemispheres. The duration of the annual fire season seems to vary between 2 and 6 months and in the tropics is highly constrained by the duration of the dry season.

There are, however, noteworthy limitations to these satellite datasets: not every fire is detected, usually related to the instruments limitations and their detection algorithm, obscuration by clouds or the limited diurnal sampling captured by the satellite orbit; and the number of fire pixels observed within a grid cell does not necessarily indicate the total area burned within the grid cell.

2.3.2 Future fire conditions and fire danger rating

Using statistical models of fire activity, fire danger rating systems are developed: these describe different characteristics of fire and are based on predicted meteorological conditions such as temperature, humidity, wind and precipitation. Fire danger can be rated in numerous ways but, in general, the higher the fire danger rating, the more dangerous the conditions. The Canadian Wildland Fire Information Systems (CWFIS) Fire Weather Index (FWI) is one of the most used fire danger indices, globally. It is a numeric rating of fire intensity, developed as a general index of fire danger for the Canadian forests, and it relies on fire spread and the total amount of fuel available for combustion [Wagner, 1987]. FWI integrates results from two other indices, namely the Initial Spread Index, a numeric rating of the expected rate of fire spread, which combines the effects of wind and fuel moisture, and the Buildup Index, which uses fuel moisture to rate the total amount of fuel available for combustion. Using the FWI, a numeric rating of the difficulty of controlling fires is estimated: the Daily Severity Rating (DSR); or its seasonal length-scaled version, the Cumulative Severity Rating (CSR).

Similarly, the McArthur Forest Fire Danger Index (FFDI) developed in McArthur [1967], uses temperature, humidity, wind and fuel availability to predict fire danger. The FFDI is widely used by the Australian Bureau of Meteorology to forecast the influence of weather on fire behaviour and, although it shows similar climatological patterns to FWI, FFDI is relatively more sensitive to temperature and relative humidity, and less sensitive to wind speed and rainfall, than FWI [Dowdy *et al.*, 2010]. FFDI's fuel availability is evaluated using the "Drought Factor", which represents the influence of recent temperatures and rainfall events on fuel availability and is partly based on the soil moisture deficit. The latter can be estimated using the Keetch-Byram Drought Index (KBDI) [Keetch and Byram, 1968], an indicator of

the soil moisture below saturation up to a maximum field capacity.

Much as the previously mentioned indices, the United States of America's National Fire-Danger Rating System (NFDRS), uses daily weather data to determine fuel moisture [Bradshaw *et al.*, 1984]. However, the NFDRS needs more input data than FWI, and whereas the latter uses a semi-empirical approach based on several decades' worth of weather, fuel moisture and test fire behaviour data, the NFDRS relies on fire spread and the physics of heat and moisture transfer [Kleschenko *et al.*, 2004]. Mölders [2010], found that both NFDRS and FWI are successful in capturing the observed variability of fire activity in the 2005 Interior Alaska June wildfires, with a slightly greater advantage for FWI than NFDRS.

Several studies have used these indices, associated with GCMs, RCMs and future scenarios, to assess future fire danger. Flannigan *et al.* [2013] used the CSR, SRES scenarios A1B, A2 and B1, and outputs from three GCMs (CGCM3.1, from the Canadian Centre for Climate Modelling and Analysis, HadCM3, from the Hadley Centre for Climate Prediction in the United Kingdom, and the IPSL-CM4 from France) to examine the potential influence of climate change on future global fire season severity. Their results suggest that significant increases in wildfire events over most of the globe may be attributed to the role temperature plays in fire activity, and that fire seasons will be more severe (in some areas of the globe, increasing by 20 days per year). Also using a CWFIS product, Moriondo *et al.* [2006] evaluated the present and future fire risk in the Mediterranean region using FWI and the output of the HadRM3P GCM along with SRES A2 and B2 scenarios. Results show that the higher risks in forest fire are due to increases in maximum temperature and decreases in precipitation and relative humidity, namely during the summer period. Liu *et al.* [2010], explored fire risk under current and future climate conditions using KBDI and climate variables simulated by four GCMs (HadCM3; CGCM2; CSIRO, from the Commonwealth Scientific and Industrial Research Organisation; and NIES, from the National Institute for Environmental Studies in Japan). The GCM simulation for the future was performed for four emission scenarios: SRES A1, A2, B1 and B2. They found that future fire potential is expected to increase significantly in the United States, South America, central Asia, southern Europe, southern Africa and Australia, i.e. mainly areas that currently have significant fire occurrence and many fire-dependent forest types. They have also found that there is an increase in fire season length, as well as a higher likelihood of extreme weather events.

Lastly, Silva *et al.* [2016] provided the basis for this dissertation where a fire danger index specifically tailored for Brazilian biomes, the Meteorological Fire Danger Index (MFDI), and the RCA4 regional climate model are used to evaluate meteorological fire danger patterns in Brazilian savannas and shrublands. Their results suggest increased likelihood of more severe fire seasons in these regions over the 21^{st} century, for an intermediate scenario of climate change (RCP4.5). In this dissertation, a more meticulous validation of both the MFDI fire danger index and the RCA4 regional climate model is performed, using several reanalysis products and a burned area dataset. Furthermore, whereas in Silva *et al.* [2016] fire danger was extrapolated for the future without calibration, here we use past climate data to calibrate the regional climate model. RCP2.6 and RCP8.5 are also analysed, as well as present and future burned area using linear regression models.

3. Data and pre-processing

3.1 Study area

The biome classification scheme used is based on the MODIS Terra and Aqua Combined Land Cover product which incorporates five different land cover classification schemes, derived through a supervised decision-tree classification method [Friedl *et al.*, 2010]. The dataset is produced yearly employing global mosaics of the standard MODIS instrument from NASA. Here, the IGBP global vegetation classification adapted by the Brazilian Centre for Weather Forecasting and Climate Studies (CPTEC) from INPE in 2005 is used.

Table 3.1: IGBP's classification scheme [Strahler *et al.*, 1996].

Vegetation class	*Description*
Evergreen Needleleaf Forests	Lands dominated by trees with a percent canopy cover $> 60\%$ and height exceeding 2 meters. Almost all trees remain green all year. Canopy is never without green foliage.
Evergreen Broadleaf Forests	Lands dominated by trees with a percent canopy cover $> 60\%$ and height exceeding 2 meters. Almost all trees remain green all year. Canopy is never without green foliage.
Deciduous Needleleaf Forests	Lands dominated by trees with a percent canopy cover $> 60\%$ and height exceeding 2 meters. Consists of seasonal needleleaf tree communities with an annual cycle of leaf-on and leaf-off periods.
Deciduous Broadleaf Forests	Lands dominated by trees with a percent canopy cover $> 60\%$ and height exceeding 2 meters. Consists of seasonal broadleaf tree communities with an annual cycle of leaf-on and leaf-off periods.
Mixed Forests	Lands dominated by trees with a percent canopy cover $> 60\%$ and height exceeding 2 meters. Consists of tree communities with interspersed mixtures or mosaics of the other four forest cover types. None of the forest types exceeds 60% of landscape.
Closed Shrublands	Lands with woody vegetation less than 2 meters tall and with shrub canopy cover is $> 60\%$. The shrub foliage can be either evergreen or deciduous.
Open Shrublands	Lands with woody vegetation less than 2 meters tall and with shrub canopy cover is between 10-60%. The shrub foliage can be either evergreen or deciduous.
Woody Savannas	Lands with herbaceous and other understorey systems, and with forest canopy cover between 30-60%. The forest cover height exceeds 2 meters.
Savannas	Lands with herbaceous and other understorey systems, and with forest canopy cover between 10-30%. The forest cover height exceeds 2 meters.

Grasslands	Lands with herbaceous types of cover. Tree and shrub cover is less than 10%.
Permanent Wetlands	Lands with a permanent mixture of water and herbaceous or woody vegetation that cover extensive areas. The vegetation can be present in either salt, brackish or fresh water.
Croplands	Lands covered with temporary crops followed by harvest and a bare soil period (e.g., single and multiple cropping systems). Note that perennial woody crops will be classified as the appropriate forest or shrub land cover type.
Urban and Built-up	Land covered by buildings and other man-made structures.
Cropland/Natural Vegetation Mosaics	Lands with a mosaic of croplands, forest, shrublands, and grasslands in which no one component comprises more than 60% of the landscape.
Snow and Ice	Lands under snow and/or ice cover throughout the year.
Barren	Lands exposed soil, sand, rocks, or snow and never has more than 10% vegetated cover during any time of the year.
Water Bodies	Oceans, seas, lakes, reservoirs, and rivers. Can be either fresh or salt water bodies.

The 1 km per 1 km grid dataset defines terrestrial biomes in 17 vegetation classes which includes 11 natural vegetation classes, 3 human-altered classes and 3 non-vegetated classes (Table 3.1).

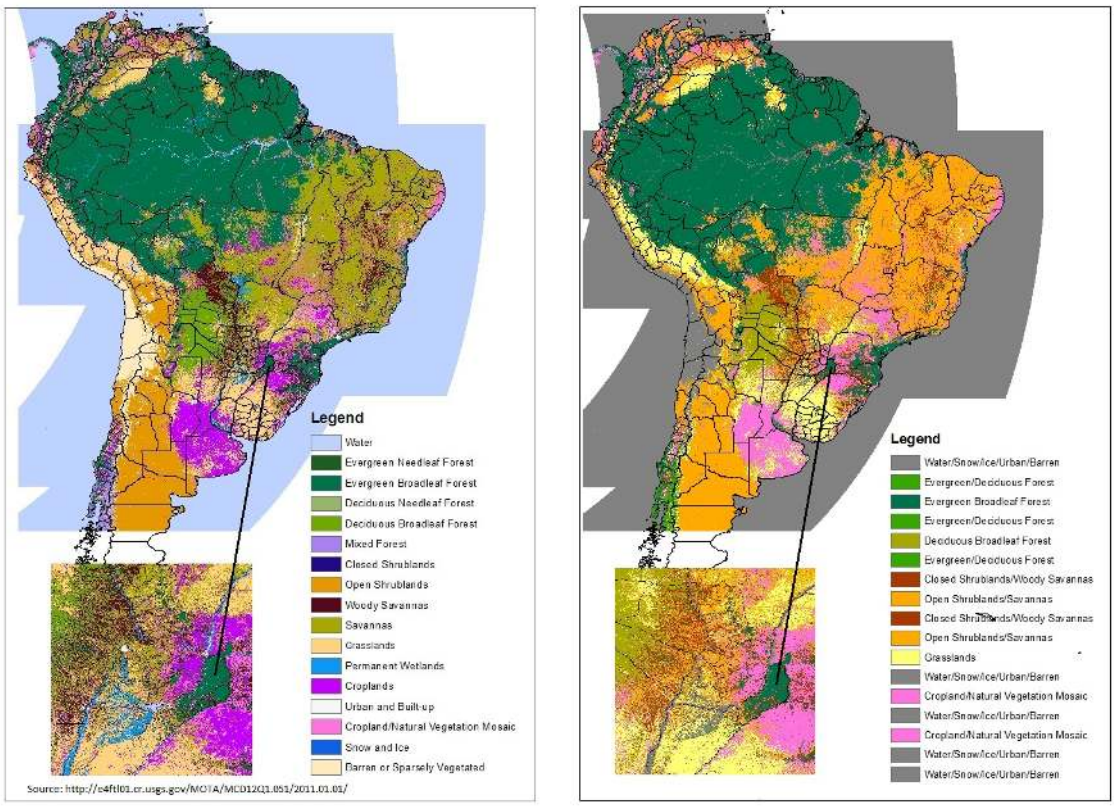

Figure 3.1: Biome distribution in South America using the IGBP vegetation scheme in 17 classes (left figure) and 7 classes (right figure) [Programa Queimadas INPE, 2013].

The IGBP nomenclature is meant to be used for all regions of the globe regardless of their particular biome characteristics. For Brazil, INPE condensed the 17 classes into 7 categories (Figure 3.1): Grasslands (*G*); Croplands (*C*); Open Shrublands and Savannas (*OS*); Closed Shrublands and Woody Savannas (*CSWS*); Evergreen Needleleaf, Deciduous Needleleaf and Mixed forests (*NLM*); Deciduous Broadleaf Forest (*DBL*); and Evergreen Broadleaf Forest (*EBL*). The *Instituto Brasileiro de Geografia e Estatística* (IBGE) adapted IGBP's classification system to the specific vegetation traits in Brazil, as shown in Table 3.2.

Table 3.2: IGBP's class number and denomination (two left columns) and correspondent IBGE's class number and denomination (two right columns) [Setzer *et al.*, 2017].

#IGBP	*IGBP's Nomenclature*	*#IGBE*	*IGBE's Nomenclature*
0	Water Bodies	0	Corpos d'água
1	Evergreen Needleleaf Forests	5	Floresta de contato; Campinarana
2	Evergreen Broadleaf Forests	7	Ombrófila densa
3	Deciduous Needleleaf Forests	5	Floresta de contato; Campinarana
4	Deciduous Broadleaf Forests	6	Florestas decíduas e sazonais
5	Mixed Forests	5	Floresta de contato; Campinarana
6	Closed Shrublands	4	Savana arbórea; Caatinga fechada
7	Open Shrublands	3	Savana; Caatinga aberta
8	Woody Savannas	4	Savana arbórea; Caatinga fechada
9	Savannas	3	Savana; Caatinga aberta
10	Grasslands	1	Pastagens e gramíneas
11	Permanent Wetlands	0	Alagados permanentes
12	Croplands	2	Agricultura e diversos
13	Urban and Built-up	0	Áreas urbanas e construídas
14	Cropland/Natural Vegetation Mosaics	2	Agriculura e diversos
15	Snow and Ice	0	Neve e gelo
16	Barren	0	Solos expostos; mineração

Since *NLM* and *DBL* categories account for only 0.4% of Brazilian vegetation, they were not considered in this analysis. Moreover, after the computation of the fire danger index, we aggregate the *CSWS* and *OS* landcovers, due to their similar ecosystem characteristics and spatial distribution.

This takes special relevance taking into account the five main brazilian biomes: *Amazónia*, *Caatinga*, *Cerrado*, *Mata Atlântica*, *Pampas* and *Pantanal*. Both *Caatinga* and *Cerrado* are mainly composed by savannas and shrublands, which represent roughly 89 and 74% of their total area respectively. *CSWS+OS* are also a significant part of *Pantanal* (57%), *Mata Atlântica* (33%) and *Pampas* (24%). Furthermore, it is also worth pointing out that 81% the Amazon rainforest is described by the *EBL* landcover.

3.2 Fire danger index

In this study we use a fire danger index specifically tailored for Brazilian biomes developed by CPTEC/INPE: the Meteorological Fire Danger Index. This index is part of the Brazilian *Programa Queimadas* and is used to calculate daily values of fire risk for South and Central America [Setzer and Sismanoglu, 2012]. Its development involved hundreds of thousands of fire events from the last decade in the most crucial Brazilian biomes.

The MFDI estimates the probability of vegetation to be burned on a given day and its rationale is

that the longer the time without rain, the higher the risk of vegetation to burn. It uses daily values of surface air temperature (T - given that the daily maximum occurs at 18:00 UTC), surface relative humidity (RH - maximum at 18:00 UTC as well), total precipitation (P) and vegetation cover. We follow the methodology proposed in Silva *et al.* [2016], in turn based on Setzer and Sismanoglu [2012]: *Risco de Fogo: Metodologia do Cálculo - Descrição sucinta da Versão 9*. A newer version has been published in 2017 with no significant changes [Setzer *et al.*, 2017].

The computation of MFDI begins with the so-called Drought Days (DD): for each given day the cumulative precipitation (mm) is estimated for eleven preceding periods of 1, 2, 3, 4, 5, 6 to 10, 11 to 15, 16 to 30, 31 to 60, 61 to 90, and 91 to 120 days. Precipitation factors are estimated considering these preceding periods, where each factor takes the form of an exponential decay and the goal is to reduce fire danger for higher volumes of rainfall in specific events and to attenuate the influence of precipitation as it occurs further in the past. Its values range from 0 to 1 and it is calculated as:

$$DD = 105 \times \prod_{i=1}^{11} e^{-\beta_i P_i} \tag{3.1}$$

where β_i and P_i are respectively the decay factor and the accumulated precipitation for period i. The range and values of such factors are described in Table 3.3.

Table 3.3: Ranges and values of the decay factors for the 11 periods that integrate the Drought Day (DD) index.

Period	**1**	**2**	**3**	**4**	**5**	**6**
Range (in days)	1	2	3	4	5	6-10
Coefficient (β)	-0.14	-0.07	-0.04	-0.03	-0.02	-0.01
Period	**7**	**8**	**9**	**10**	**11**	
Range (in days)	11-15	16-30	31-60	61-90	91-120	
Coefficient (β)	-0.008	-0.004	-0.002	-0.001	-0.0007	

The Drought Days are then used to calculate the so-called Base Danger (BD) that aims to combine the effect of rainfall with a sinusoidal curve that represents the effects of phenology for the vegetation types used in this study.

$$BD = 0.45\{1 + sin[min(A \times DD, 180^\circ) - 90^\circ]\} \tag{3.2}$$

where the argument of the sinus function is in degrees and the values of coefficient A are described in Table 3.4.

Table 3.4: Values of A for the seven types of vegetation.

Vegetation type	***EBL***	***DBL***	***NLM***	***CSWS***	***OS***	***C***	***G***
A	1.5	1.72	2	2.4	3	4	6

Figure 3.2 represents the evolution of Base Danger as the Drought Days increase for each vegetation type. The sinusoidal curves have 0.9 as their maximum value hence the limitation to 180° in Equation 3.2. It is clear that the biomes respond quite differently to the lack of precipitation: in Grasslands and Croplands, vegetation dries quickly and reaches its peak at only 30 and 45 days without rain; on the contrary, Deciduous and Evergreen Broadleaf Forests, given their typically humid and high temperature

characteristics, need much more DD so achieve maximum BD. The Amazon rainforest would be in these conditions, reaching its maximum Base Danger value at 120 days without precipitation.

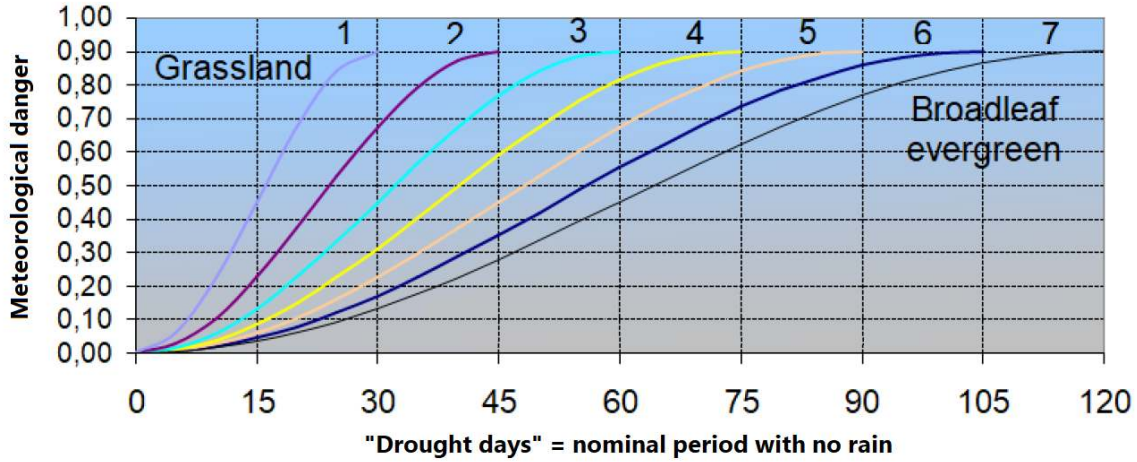

Figure 3.2: Sinusoidal curves of BD (y-axis) evolution over the Drought Days (x-axis) for the 7 vegetation types (adapted from Setzer *et al.* [2017]).

Temperature and relative humidity are taken into account by estimating the temperature (TF) and humidity factors (HF).

$$TF = T \times 0.02 + 0.4 \tag{3.3}$$

$$HF = RH \times -0.006 + 1.3 \tag{3.4}$$

Lastly, MFDI is calculated multiplying the Base Danger by the above-mentioned factors.

$$MFDI = BD \times TF \times HF \tag{3.5}$$

It is worth noting that this methodology does not consider wind speed because it regards fire spread.

3.3 Climate reanalyses

The observation-based data for the period 1980-2016, comprehends the European Centre for Medium-Range Weather Forecasts (ECMWF) ERA-Interim reanalysis [Dee *et al.*, 2011], the NOAA/NCEP NCEP-DOE Reanalysis 2 [Kanamitsu *et al.*, 2002], and NASA/GMAO MERRA-2 reanalysis [Gelaro *et al.*, 2017] (Table 3.5).

- ERA-Interim (henceforth referred as ERA-I) uses the ECMWF Integrated Forecast Model (IFS Cy31r2) and the data assimilation scheme is based on a 12-hourly four-dimensional variational analysis (4D-Var). Its spectral resolution is T255, using 60 vertical levels with the top of the atmosphere at 0.1 hPa, and a resolution of $0.125° \times 0.125°$.
- NCEP-DOE's (NCEP) model is identical to the NCEP global spectral model operational in 1995, except with a spectral resolution of T62 and 28 vertical model layers. Its analysis scheme is a 6-hourly three-dimensional variational (3D-Var), ad it has a spatial resolution of $1.875° \times 1.875°$.

- MERRA-2 (MERRA) uses the new and improved version of the Goddard Earth Observing System data assimilation system version 5 (GEOS-5), based on a 6-hourly three-dimensional variational (3D-Var), with a resolution of $0.5^\circ \times 0.625^\circ$ and 72 vertical levels from the surface to 0.01 hPa.

These three reanalysis datasets produce varying results according to their different data assimilation schemes, providing a range of admissible results which allows to better assess and validate the regional climate model. Moreover, several studies have explored the differences between these reanalyses and how their respective physical processes are described (e.g. Trenberth *et al.* [2011], Brunke *et al.* [2011] and Bosilovich *et al.* [2008]).

Both ERA-I and MERRA are updated in near real-time, with monthly delay due to production and validation of data, whereas NCEP-DOE is updated in real-time (only few days behind). All data was selected for South America (coordinates of upper left and lower right corners: N20 W-90 and S-60 E-30).

Table 3.5: Retrieved datasets and correspondent units.

ERA-Interim	2 Metre dew point temperature	K
	2 Metre temperature	K
	Total precipitation	mm/day
NCEP-DOE R2	Air temperature	K
	Specific Humidity	kg/kg
	Precipitation rate	$kg/m^2/s$ = mm/s
	Pressure	Pa
MERRA-2	Surface Temperature	K
	Humidity	kg/kg
	Precipitation rate	$kg/m^2/s$ = mm/s
	Surface Pressure	Pa

Simple conversions are then performed to match the reanalyses' dataset units to those used in MFDI calculation. None of the reanalyses provided relative humidity values. As such, two methodologies were used to calculate relative humidity using the available parameters in each reanalysis. ERA-I uses the Magnus formula [Lawrence, 2005] to estimate water vapor pressure (e) and the saturation vapour pressure (e_s) using surface (T) and dew point temperatures (T_d):

$$e = C_1 exp\left(\frac{A_1 \times T_d}{B_1 + T_d}\right) \tag{3.6}$$

$$e_s = C_1 exp\left(\frac{A_1 \times T}{B_1 + T}\right) \tag{3.7}$$

$$RH = 100 \times \frac{e}{e_s} \tag{3.8}$$

where $A_1 = 17.625$, $B_1 = 243.04$°C and $C_1 = 6.1094$ hPa. These values, suggested by Alduchov and Eskridge [1996], provide results for e and e_s with a relative error of $< 0.4\%$ over the range $-40°C \leq T \leq 50°C$. Relative humidity can then be calculated using both these results (Equation 3.8).

On the other hand, for both NCEP-DOE and MERRA, relative humidity is calculated using specific humidity (q), surface pressure (p) and temperature (T). Another definition of RH uses the actual water vapour dry mass mixing ratio (w) and the saturation mixing ratio (w_s) at ambient temperature and pressure:

$$RH = 100 \times \frac{w}{w_s} \tag{3.9}$$

For must purposes specific humidity is approximated by the mixing ratio, as the amount they differ is less than the error involved in measuring either of them [Oliver, 2005]. Also, the saturation mixing ratio (w_s) is calculated using the saturation vapour pressure and surface pressure:

$$w_s = \frac{\varepsilon \times e_s}{p - e_s} \approx \frac{\varepsilon \times e_s}{p} \tag{3.10}$$

where $\varepsilon = 0.622$ represents the ratio of the molecular weights of water and dry air. As the saturation vapour pressure is substantially lower than the total mass, the denominator or the previous equation can be simplified to p. Finally, from Equation 3.9 we can replace the e_s by its definition:

$$RH = \frac{q}{\frac{0.622 e_s}{p}} \times 100 = \frac{pq \times 100}{0.622 e_s} = \frac{pq \times 100}{0.622 \times 6.1094 \times exp(\frac{17.625 \times T}{T+243.04})} = \frac{263.2 \times pq}{exp(\frac{17.625 \times T}{T+243.04})} \tag{3.11}$$

3.4 Regional climate model output

The regional climate is simulated by the regional downscaling of EC-Earth for the South American domain of the CORDEX experiment, performed by the Rossby Centre using their atmospheric model, the RCA4 [Strandberg *et al.*, 2015]. The EC-Earth is a coupled global climate model based on the operational seasonal forecast system of the ECMWF [Hazeleger *et al.*, 2012], used in the Coupled Model Intercomparison Project Phase 5 (CMIP5). EC-Earth outputs were used as boundary condition for the RCA4 regional climate model, which includes improved land surface processes, such as the lake model and physiography compared to its older version [Samuelsson *et al.*, 2015]. RCA4 is based on the numerical weather prediction model HIRLAM and is thoroughly described in Samuelsson *et al.* [2011]. It is worth noting that the regional model's mask for the land-sea and the fractions of lakes/forests remains static throughout the calculations. Both regional and global climate models have shown satisfactory results in representing several components of the climate system, in particular the ones relevant for this study: EC-Earth has been shown to satisfactorily replicate the ocean component compared to observations [Sterl *et al.*, 2012]; further comparisons with observational-data in the Nordic and Baltic Seas [Dieterich *et al.*, 2013], the Arctic [Koenigk *et al.*, 2013] and South Asia [Iqbal *et al.*, 2017] have also yield satisfactory results.

Daily values of near-surface air temperature, near-surface relative humidity and precipitation were obtained at a spatial resolution of $0.44^\circ \times 0.44^\circ$ (approximately 50 km) for the South America domain (SAM-44, with rotated coordinates N34.76 W143.92 S-38.28 E207.72). Four distinct experiments were used, one corresponding to the historical period for model and index validation (1980-2005), and the others corresponding to IPCC's RCPs 2.6, 4.5 and 8.5 for the 21^{st} century [IPCC, 2013]. RCPs 2.6, 4.5 and 8.5, correspond, respectively, to a stringent mitigation, mild and severe climate change scenarios; the first being the closest to the 1.5°C above pre-industrial levels goal set in the COP21 meeting in Paris, December 2015 [UNFCCC, 2017].

3.5 Burned area

To estimate burned area we used the *Área Queimada* burned-area product at 1 km resolution developed by Libonati *et al.* [2015] specifically for Brazil. The dataset is a matrix of 0 (not burned) and 1 (burned area). Given that the computational capability needed to run the AQM data at its original resolution is beyond the available material's (more than 24 hours a run), the dataset had to be projected to a coarser resolution, namely ERA-I's. To that end, latitude and longitude values were selected and, per each lat-lon combination of the coarser resolution, the amount of burned pixels (value = 1) in the thinner AQM grid are added to a total burned area value over each new lat-lon combination. Therefore, we have a new matrix in $0.125^\circ \times 0.125^\circ$ resolution with total burned area per pixel, with values ranging from 0 to 169 (in km^2).

3.6 Pre-processing

Daily values of observation-based MFDI are computed for 1981-2016 at each grid point using temperature, relative humidity and precipitation data from the three reanalyses (ERA-I, MERRA and NCEP) and taking into account the assigned land cover type as derived from the modified IGBP map using the nearest neighbour criterion. For each reanalysis dataset, monthly mean values of observed-based MFDI were obtained for *EBL*, *CSWS+OS*, *C* and *G* by averaging gridded daily values over each month and then by spatially averaging over grid points belonging to same vegetation type.

The same procedure was applied to simulation-based MFDI from the RCA4 model in order to obtain the respective monthly mean values for each main vegetation type for the historical period (1976-2005) and for RCPs 2.6, 4.5 and 8.5, in two 30-year periods, ending in the first half (2021-2050) and in the second half (2071-2100) of the 21^{st} century.

BA data is similarly processed to MFDI, however instead of spatially averaging the grid points correspondent to the same vegetation, these were aggregated.

All fire danger datasets, both reanalyses and RCM, are used in their native resolution. We compare aggregated and averaged values over the different spatial resolutions which, although it might lead to small incongruities, avoids errors from resampling. Lastly, a mask of Brazil was computed and reprojected to the used resolutions using nearest neighbour interpolation as well.

4. Methods

Burned area models are built for each main vegetation type by means of linear regression analysis performed on time series of MFDI (predictor) and BA (predictand). Performance of fitted models was compared based on the coefficient of determination, providing information about the goodness of fit. Given the short length of the time series, effects of overfitting were assessed using a leave-one-out-cross validation scheme [Wilks, 1995], which evaluates the models' predictive ability using non-evaluated data: the model is fit to the data using all but one observation, then the unused observation is estimated with the resulting model. This methodology is applied for the 12 years of data (2005-2016), leaving 1 year aside each iteration.

Using the maximum likelihood method, normal models are fitted to the distributions of several MFDI time series for the different landcovers and the Lilliefors test [Lilliefors, 1967] is used to test the null hypothesis that data come from a normally distributed population with mean and standard deviation. Lilliefors test for normality is based on the Kolmogorov-Smirnov test, for mean and variance unknown or derived from the sample, the latter being the current situation. Mean, standard deviation and their associated confidence intervals (at a 95% confidence level) are also estimated.

Finally, following Pereira *et al.* [2013], a variable X_1 with normal distribution and mean μ_1 and standard deviation σ_1 is converted into a variable X_2 with normal distribution and mean μ_2 and standard deviation σ_2. As such, when applying to the simulation-based fire danger ($MFDI_{sim}$) and the observational-based data ($MFDI_{obs}$):

$$X = \frac{MFDI_{sim} - \mu_1}{\sigma_1} \sim N(1,0) \tag{4.1}$$

Given that $X \sim N(1,0)$:

$$MFDI_{obs} = \sigma_2 X + \mu_2 \sim N(\mu_2, \sigma_2) \tag{4.2}$$

Using both of these, $MFDI_{sim}$ is approximated to $MFDI_{obs}$ using the following transformation:

$$\begin{aligned}
&MFDI_{obs} = \sigma_2 X + \mu_2 \sim N(\mu_2, \sigma_2) \Leftrightarrow \\
&MFDI_{obs} = \sigma_2 \frac{MFDI_{sim} - \mu_1}{\sigma_1} \sim N(\mu_2, \sigma_2) \Leftrightarrow \\
&MFDI_{obs} = \frac{\sigma_2}{\sigma_1}\left(MFDI_{sim} - \mu_1 + \frac{\sigma_1}{\sigma_2}\mu_2\right) \sim N(\mu_2, \sigma_2) \Leftrightarrow \\
&MFDI_{obs} = \frac{MFDI_{sim} - (\mu_1 - \frac{\sigma_1}{\sigma_2}\mu_2)}{\frac{\sigma_1}{\sigma_2}} \sim N(\mu_2, \sigma_2)
\end{aligned} \tag{4.3}$$

5. Results

5.1 Observation-based data

5.1.1 Seasonal cycle

For each vegetation type, the respective annual cycles of MFDI and of BA for the 12-year period (2005-2016) are computed by averaging for each month the respective monthly means over the considered period. As shown in Figure 5.1, the annual cycles of MFDI for all vegetation types present a pronounced maximum in winter (August-October), with the largest values being attained for *CSWS+OS* and the lowest for *EBL*. BA follows similar trends, also achieving its highest values in *CSWS+OS* (monthly maximum of 13.5 $\times$ 10 000 km^2 in September) and lowest in *EBL* (maximum at 0.77 $\times$ 10 000 km^2 in September).

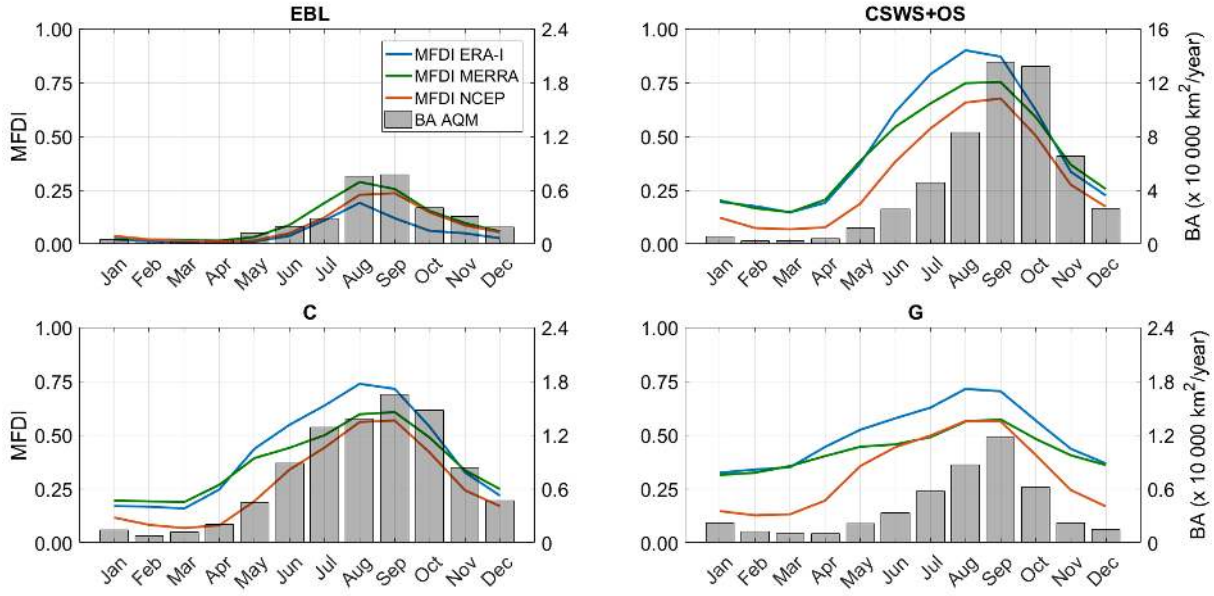

Figure 5.1: Annual cycles of MFDI (solid curves) and of burned area (bars) for the four main vegetation types during the period 2005-2016. Annual cycles of MFDI are derived from ERA-I (blue curve), MERRA (green curve) and NCEP (orange curve), whereas the annual cycle of burned area is based on the AQM product.

There are systematic differences among the annual cycles of MFDI of the three reanalyses, *EBL* and the remaining three vegetation types presenting a contrasting behaviour along the year. Whereas in *EBL* the MERRA reanalysis presents the higher values of MFDI, ERA-I the lowest, and NCEP has values close to ERA-I from May to August and close to MERRA from September to December, the same is not true in the other vegetation types. In these, ERA-I achieves the highest values, NCEP the lowest and MERRA presents intermediate values from May to October and is close to ERA-I in the remaining months. During the period of larger values of MFDI, from July to October, the contrast is more pronounced when comparing ERA-I and the other two reanalyses, with ERA-I presenting lower values in *EBL*, and higher in the remaining vegetation types.

This feature may be traced back to differences between the annual cycles of the meteorological parameters of the three reanalyses. Figure 5.2 shows the annual cycles for *EBL* and *CSWS+OS* (similar behaviour being observed in *C* and *G*): the ERA-I reanalysis presents systematic higher (lower) values of temperature (relative humidity) along the year in both *EBL* and *CSWS+OS* but the same is not true for the annual cycle of precipitation where ERA-I has higher values in *EBL* (in particular between July and October) and intermediate values in *CSWS+OS*.

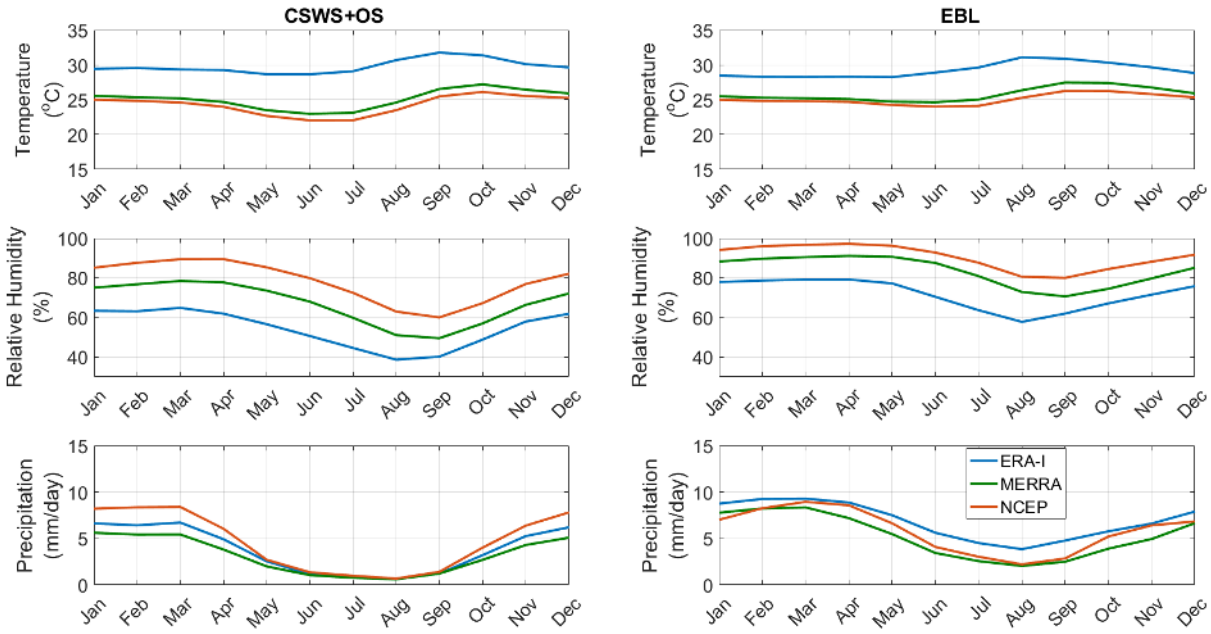

Figure 5.2: Annual cycles of temperature, relative humidity and precipitation for *CSWS+OS* and *EBL* during the period 2005-2016 as derived from ERA-I (blue curve), MERRA (green curve) and NCEP (orange curve) reanalyses.

For *EBL*, the annual cycle of BA is in close agreement with that of MFDI (Figure 5.1), both cycles presenting the highest values in August and September. However, in the cases of *CSWS+OS* and *C*, the highest BA values occur in September and October, one month after the highest values of MFDI, in August and September. The same delay of one month is observed with the peak of BA in *G* that takes place in September. This might be due to its vegetation accumulating stress in the highest fire danger months (i.e. hot and dry) and therefore being more prone to burn afterwards.

Comprising about 39% of the Brazilian territory, *CSWS+OS* contributed with 647 thousand hectares (10^4 km^2) of BA representing 76% of the total BA amount (849 thousand hectares) during the period 2005-2016 (Table 5.1). In the case of *EBL*, although representing 42% of the area of Brazil, its BA of 38 thousand hectares only represents 4% of the total BA. *C* (*G*), representing 11% (4%) of the area of Brazil contributed with 108 (56) thousand hectares, corresponding to 13% (7%) of the total BA.

Moreover, 62% of the total BA is due to events taking place from August to October; half of the events in *CSWS+OS* take place in September-October and almost half (48%) of events in *EBL* occur in August-September, whereas *G* and *C* present more even distributions from August to October. It is worth noting that *G* and *C* are highly susceptible to anthropogenic activity, and thus these results suggest focusing on the highest burning period for natural biomes, i.e. on August to October, hereafter referred to as the fire season.

Table 5.1: Total BA recorded during 2005-2016 for each main vegetation type and relative contributions of August, September and October to the total amounts.

Vegetation type	**Total BA** ($\times$ 10 000 km^2)	**Contribution (%) to Total BA**			
		August	**September**	**October**	**Total**
EBL	38	24	24	13	61
CSWS+OS	647	15	25	25	65
C	108	15	18	17	50
G	56	19	25	13	57
All	**849**	**16**	**24**	**22**	**62**

5.1.2 Interannual variability

For each year and vegetation type, the fire season was characterized by the mean values of MFDI (for each reanalysis) and of BA as obtained by averaging the respective monthly values in August, September and October. As shown in Figure 5.3, for all vegetation types the inter-annual variability of BA in the fire season correlates well with the inter-annual variability of MFDI, the larger (smaller) values of BA matching higher (lower) values of MFDI. Systematic differences among the inter-annual variability of MFDI from the three reanalyses are similar to those already mentioned for the annual cycles, values from ERA-I being the largest in all years for *CSWS+OS*, *C* and *G* and NCEP presenting the lowest values in most of the period; for *EBL*, MFDI from ERA-I achieves lowest values in all but one year, and MFDI from MERRA is the largest in all except the first four years.

Still, not all peaks in BA correspond to high MFDI, most likely due to anthropogenic influence on burned area in those years, seeing as fire ultimately depends on ignition.

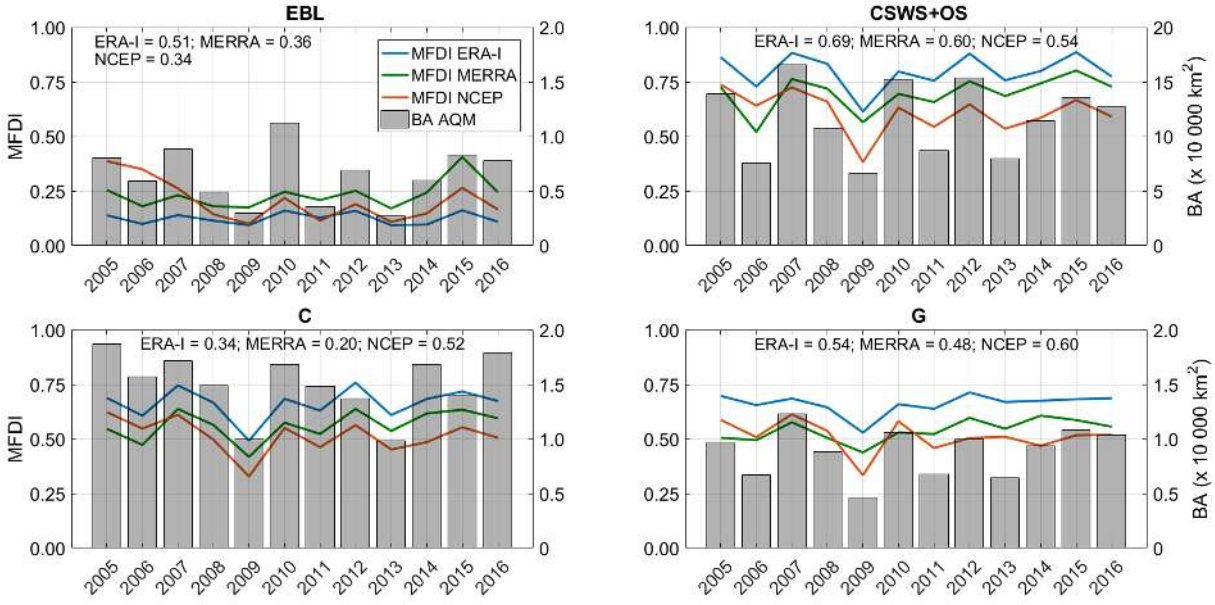

Figure 5.3: Inter-annual variability, for the four main vegetation types during the period 2005-2016, of the mean values over the fire season (August to October) of BA (bars) and MFDI (solid curves) as derived from ERA-I (blue curve), MERRA (green curve) and NCEP (orange curve) reanalyses. The coefficients of determination between BA and MFDI from the three reanalyses are shown at the top of each panel.

Values of the coefficient of determination between BA and MFDI from the three reanalyses are also shown in Figure 5.3 and it is worth noting that, for each vegetation type and for different reanalysis

products, at least half of the variance of BA is predictable from MFDI. When using ERA-I, values of the coefficient of determination for *CSWS+OS* and *EBL* are well above those obtained with the other reanalyses, reaching 0.69 in *CSWS+OS* and 0.51 in *EBL*. In the case of *C* and *G*, the coefficient of determination is lower using ERA-I, 0.34 and 0.54 respectively; the largest values, 0.52 and 0.60, are obtained when using MFDI from NCEP.

The BA and MFDI results achieved for *EBL*, allow to establish a relation with the extreme events registered from 2005-2016 in the Amazon rainforest: the 2009 extreme flooding [Filizola *et al.*, 2014] is accompanied by a decrease of BA and MFDI (except for MERRA, due to a more pronounced increase in RH and decrease of P in that year); followed by the 2010 one-in-a-century drought [Marengo *et al.*, 2011] and a surge in BA as well as in MFDI; lastly, in 2015 there is a sudden increase in burned area and MFDI possibly due to the 2015 severe drought associated with El-Niño conditions [Panisset *et al.*, 2018].

5.2 Burned area models

Results obtained in the previous section suggest building linear regression models where MFDI is used to predict BA during the fire season. The largest values of the coefficient of determination that were obtained using MFDI from ERA-I ($MFDI_{ERAI}$) in the two most relevant vegetation types (*CSWS+OS* and *EBL*, representing 82% of the area of Brazil) and the finer spatial resolution of ERA-I data justify choosing $MFDI_{ERAI}$ as the predictor.

For each vegetation type, linear models were built using $MFDI_{ERAI}$ as the predictor and BA_{AQM} as the predictand. Models were fitted using means for each month of the fire season (August, September and October), means over two months (August-September and September-October) and means over the entire fire season (i.e. the same models already used to analyse the interannual variability of MFDI and BA). Performance of each fitted model is assessed based on values of coefficient of determination before and after a leave-one-out cross validation scheme (Table 5.2) that respectively give information about goodness of fit and effects of overfitting.

Table 5.2: Coefficients of determination between BA_{AQM} and $MFDI_{ERAI}$ for linear models and main vegetation types based on averages over one month (August, September and October), two months (August-September and September-October) and the fire season (August to October). Values in parenthesis are those obtained after cross-validation. Chosen model for each vegetation type is highlighted in bold.

Vegetation type	August	September	October	August - September	September - October	Fire season
EBL	0.58	0.37	0.32	0.43	0.44	**0.51**
	(0.44)	(0.15)	(0.17)	(0.19)	(0.28)	**(0.33)**
CSWS+OS	0.45	0.43	0.79	0.46	**0.77**	0.69
	(0.24)	(0.22)	(0.72)	(0.27)	**(0.68)**	(0.58)
C	0.17	0.46	0.65	0.15	**0.63**	0.34
	(0.02)	(0.27)	(0.53)	(0.01)	**(0.48)**	(0.09)
G	0.29	0.41	0.66	0.37	**0.66**	0.54
	(0.11)	(0.14)	(0.53)	(0.14)	**(0.46)**	(0.44)

In the case of models based on monthly means, the largest values of the coefficients before and after cross-validation are obtained in August for *EBL* (0.58 and 0.44) and in October for the remaining three vegetation types: *CSWS+OS* (0.79 and 0.72), *G* (0.66 and 0.53) and *C* (0.65 and 0.53). For models

based on two-month averages, the largest values of the coefficient of determination occur in September-October for all vegetation types, ranging from 0.44 and 0.28 in *EBL*, up to 0.77 and 0.68 in *CSWS+OS*, with values of 0.63 and 0.48 in *C*, and of 0.66 and 0.46 in *G*. For averages over the fire season results, as already pointed at the end of the previous section, *CSWS+OS* presents the largest values (0.69 and 0.58), followed by *G* (0.54 and 0.44), *EBL* (0.51 and 0.33) and *C* (0.34 and 0.09). It is worth noting that models for *CSWS+OS* are best performing in all three types of averages, presenting higher values of coefficients of determination (before and after cross-validation) in October, September-October and the fire season than the respective models for the other types of vegetation. This is especially important given that *CSWS+OS* contributed to 76% of the BA in Brazil in 2005-2016 and that almost two thirds of that amount (65%) are due to events occurring during the fire season (Table 5.1).

Results for September-October are more robust given the small difference between the coefficients of determination before and after cross-validation. As such, these results suggest that the most appropriate models to study inter-annual variability of BA in *CSWS+OS*, *G* and *C* are the ones based on averages over September-October; whereas *EBL* is based on averages over the entire fire season (August to October). This choice represents a compromise between quality of fit and moderate effects of overfitting, and the relative contribution to BA that occurs in this period, respectively 50% for *CSWS+OS*, 38% for *G* and 35% for *C* (Table 5.1). In the case of *EBL*, the model based on averages over the fire season is the most appropriate, given that events taking place in the chosen period contribute to 61% of the BA in that vegetation type. Results obtained with the chosen models are shown in Figure 5.4, that allow a visual assessment of the performance of the models by comparing the observed values of BA with the modelled values using cross-validation.

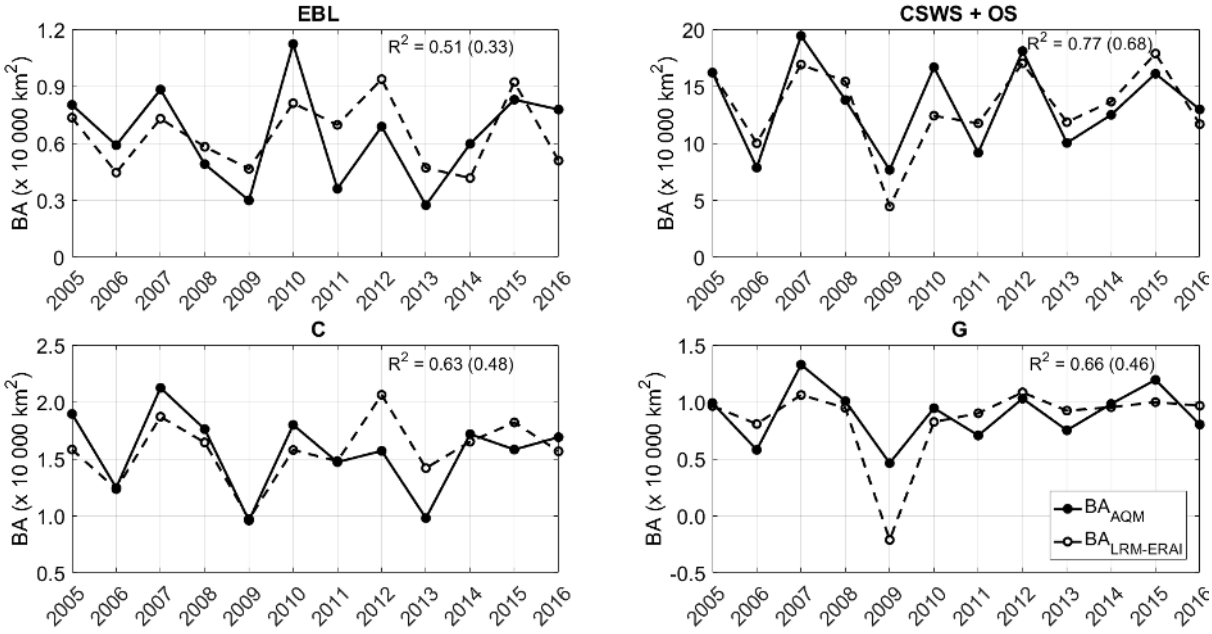

Figure 5.4: Observed burned area values from AQM (BA_{AQM}, solid curves) and respective modelled values with cross-validation of BA over 2005-2016 using the selected linear regression models for each vegetation type ($BA_{LRM-ERAI}$, dashed curves). Coefficients of determination are shown for BA_{AQM} and $MFDI_{ERAI}$ and, in parenthesis, for BA_{AQM} and $BA_{LRM-ERAI}$.

Results from Table 5.2 are consistent with the higher dependability of *CSWS+OS* to meteorological conditions, whereas in *EBL* the correlation presents a lower value suggesting a weaker dependency on meteorological fire danger. For *G*, the cross-validated results present a negative burned area in 2009,

which illustrates that, although the results are quite positive, caution is needed when applying these linear regression models.

Lastly, the linear regression coefficients m, b and R^2, were also analysed in the cross-validation results. Across all years, m, b and R^2, values stay reasonably stable for all biomes, with the exception of 2009 for G and *CSWS+OS*, and 2012 for C and *EBL*, where there was a sudden increase in m and decrease in b. The resulting R^2 values, however, did not show any major variation. This further confirms the adequacy of the burned area model to accurately replicate burned area results.

5.3 Simulated data

5.3.1 Meteorological variables

In this subsection, the capability of the RCA4 regional climate model to reproduce current climate conditions in Brazil was evaluated. A preliminary analysis on the seasonal cycle of the meteorological variables was performed: overall, the model satisfactorily replicates the seasonal cycles of precipitation, relative humidity and temperature, over the 25-year period (1981-2005) for all vegetation types.

Although the model seems to follow the same trends as the reanalyses products in *EBL* (Figure 5.5), there are considerable differences in T and P. Only the RH estimates are in the range of the observation-based products. The model estimates a marked decrease in RH from June to November (peaking in August-September) accompanied by an increase of T in the same period (with its peak in September). This seems to be in accordance with the reanalyses' results, although they appear of less magnitude. The model also estimates an increase in T from January to April that is not seen in the reanalyses, which keep steady values of, approximately, 25°C (MERRA and NCEP) and 28°C (ERA-I) for that period. A sudden increase in P from February to April is also not seen in the observation-based products, even though they also estimate a small increase in P from January to April. From April to October (which encompasses our fire season) the model underestimates P, and overestimates from October to the end of the calendar year.

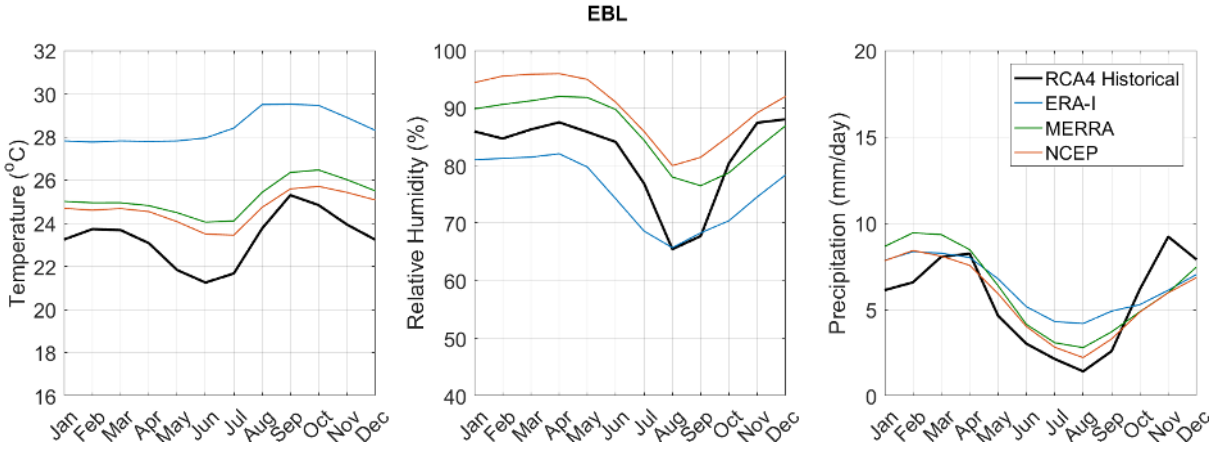

Figure 5.5: Seasonal cycles of temperature (left panel), relative humidity (centre panel) and precipitation (right panel) for *EBL*, using the historical results (1981-2005) from the RCM (black curve), ERA-I (blue curve), MERRA (green curve) and NCEP (orange curve).

As for *CSWS+OS* (Figure 5.6), similarly to *EBL*, the model keeps underestimating T compared to all observation-based products, however it shows similar trends to those seen in the reanalyses. A pronounced decrease from April to July is seen in the RCM and both MERRA and NCEP, and, although

it also estimates a decrease, ERA-I results are of much lesser magnitude. Estimated RH and P show similar trends, and they mostly stay within the observation-based data range.

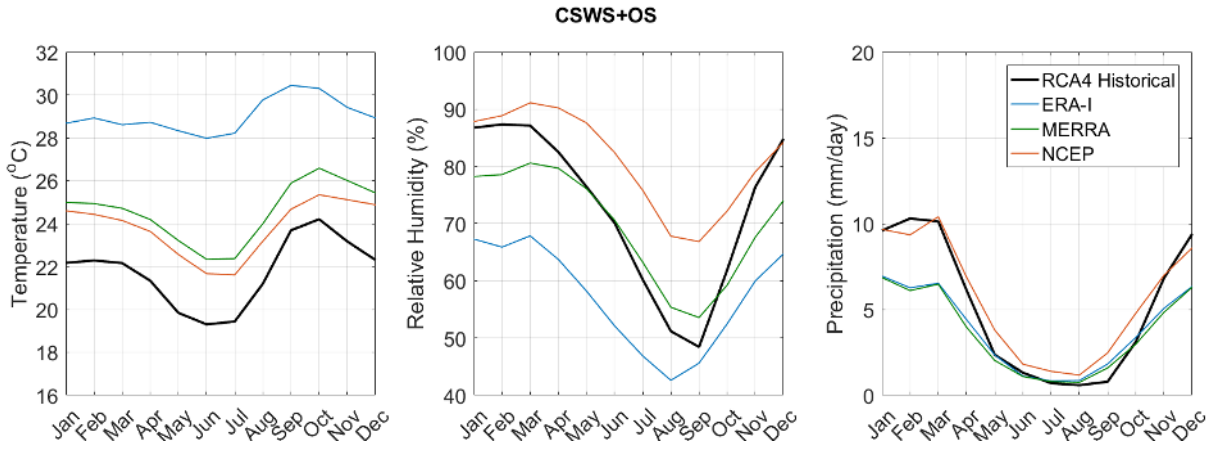

Figure 5.6: As in Figure 5.5 but regarding *CSWS+OS*.

The RCM underestimates P from May to October for *C* (Figure 5.7), which includes our fire season months, but otherwise keeps within the observation-based results range. Similarly to previous outcomes the model underestimates T, and RH values are within the expected range.

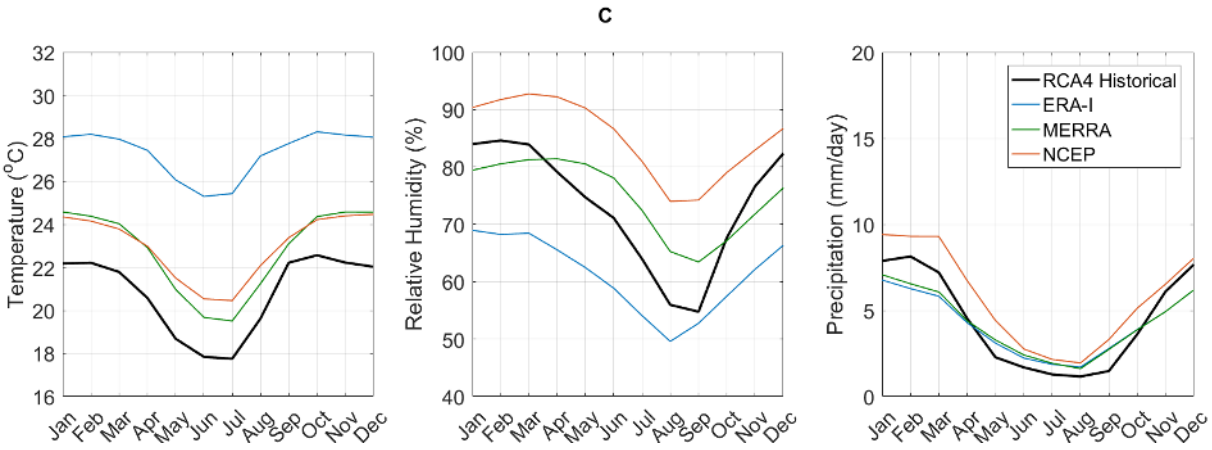

Figure 5.7: As in Figure 5.5 but regarding *C*.

Finally, for *G* (Figure 5.8), conversely to the other biomes, simulated T is quite close to MERRA's estimations, although it is still underestimated. There is a decrease in RH from March onwards that is in accordance with ERA-I results, but different to those from NCEP, which shows a small increase, and MERRA, which continues on increasing until May. Moreover, its lowest value occurs in September consistent with NCEP and MERRA results. As for P, the model follows similar trends to NCEP and underestimates from April to November.

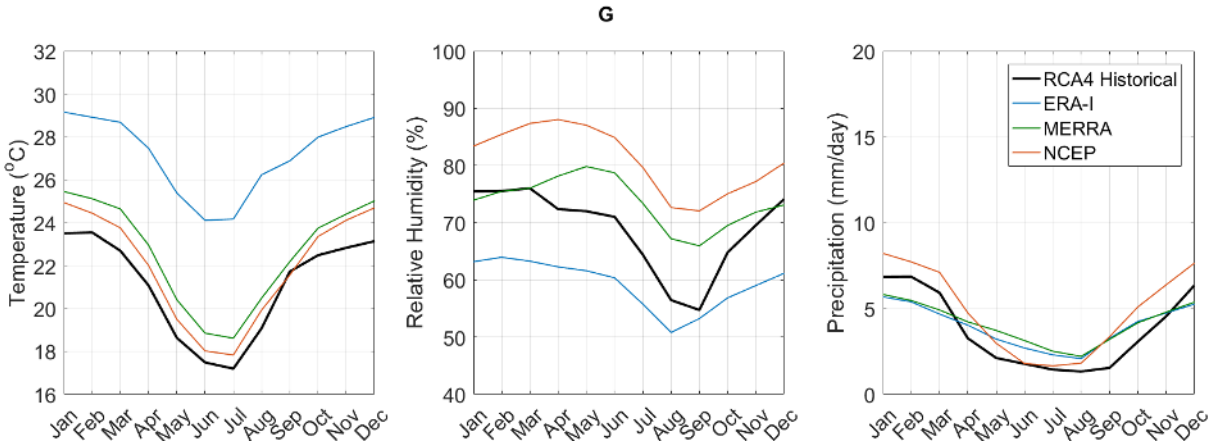

Figure 5.8: As in Figure 5.5 but regarding *G*.

5.3.2 Seasonal cycle of present and future MFDI

Using the same approach as with the observation-based data, the annual cycles of simulation-based MFDI by the RCA4 model were computed for each main vegetation type for the 1976-2005 historical period and the for all climate scenarios (RCP2.6, RCP4.5 and RCP8.5) in 2021-2050 and 2071-2100 (Figure 5.9). The annual cycles of the observation-based MFDI (from ERA-I, MERRA and NCEP reanalyses) for the period 1981-2005 are also shown for reference, conveying an indication of the uncertainty of observed climate.

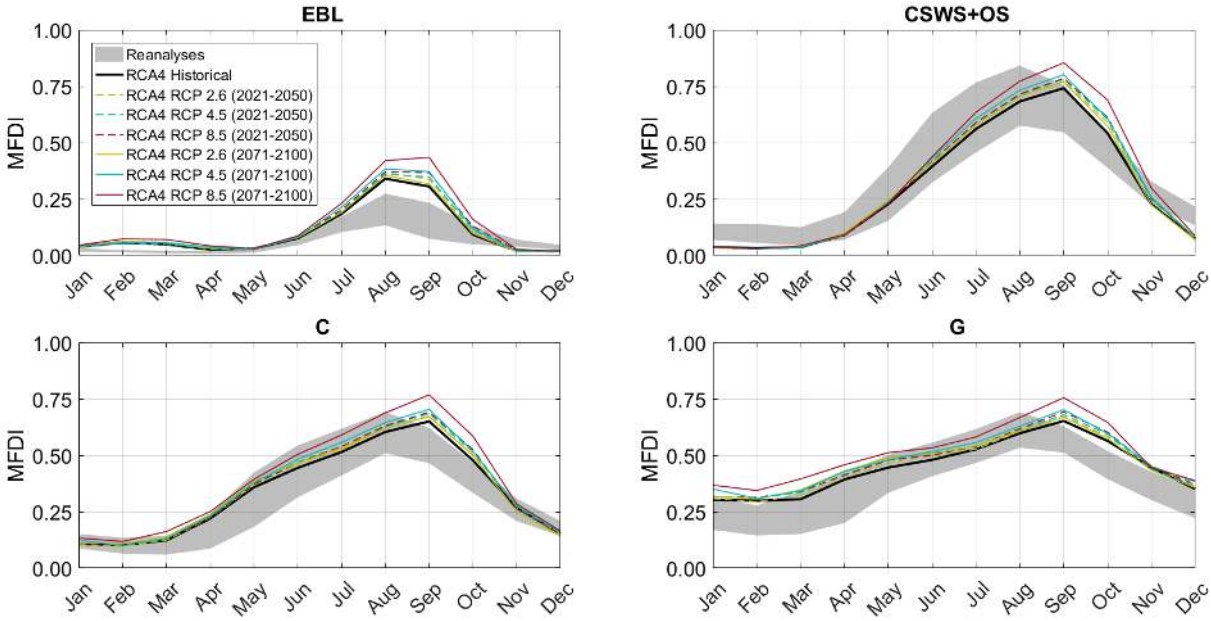

Figure 5.9: Annual cycles of simulation-based MFDI by the RCM for the historical period (1976-2005) (solid black curve) and for RCP2.6 (yellow curves), RCP4.5 (blue curves) and RCP8.5 (red curves) for both future time periods considered: 2021-2050 (dashed) and 2071-2100 (solid). Grey area represents the observation-based MFDI range from the three reanalyses, for reference.

Overall, the simulation-based MFDI follows the trends of observation-based MFDI results, staying within the reanalyses' range in most months, for all vegetation types. In *EBL*'s fire season, however, there is a marked difference between the MFDI calculated by the RCM and the three reanalyses: in August

and September the fire danger is overestimated by the model, which is in accordance with the more pronounced decrease in precipitation (right panel of Figure 5.5). The RCM also overestimates MFDI from January to April, which confirms precipitation's key role in fire danger assessment: although ERA-I presented the highest temperature and lowest relative humidity in these months, the model still calculated a much higher MFDI in that period, which can only be due to the considerable lower values of simulated P. This role has also been discussed in Libonati *et al.* [2015], where it is shown that *cerrado*'s (part of *CSWS+OS* landcover) inter-annual BA variability is closely related to annual mean total precipitation.

Like the reanalyses, simulated data has an annual cycle with a marked peak in winter. However, in *CSWS+OS*, *C* and *G*, the peaks in annual cycles of simulation-based MFDI occur in September, whereas the peaks in observation-based cycles take place one month earlier, in August. In *EBL* the observation-based and the simulated annual cycles present a peak in August, except the most severe climate scenario where the maximum of the annual cycle occurs in September. Thus, the model calculates highest fire danger in the months that burn the most, which could mean that the model is not able to properly simulate the increase in fire danger in the months prior to the burn. However, the RCM also calculates high MFDI in the preceding months with similar trends to those in reanalyses'. Consequently, although the highest fire danger month is "delayed" compared to the observation-based products, the model can still accurately predict higher MFDI in the fire season.

For all vegetation types, the simulated annual cycles of MFDI for future climate scenarios show a systematic increase along the year, that is largest during the fire season, when going from RCP2.6, to RCP4.5 up to RCP8.5. The annual cycle for the mildest (most severe) future climate scenario defines the lower (upper) bound of simulated intra-annual variability of MFDI in future climate scenarios. For scenarios RCP4.5 and RCP8.5, there is a systematic increase in the annual cycle from 2021-2050 to 2071-2100. This is not the case in scenario RCP2.6, where there is a small decrease in MFDI when going from the first 30-year period to the second one. In 2021-2050, for each vegetation type, the annual cycles of MFDI for all RCPs are very close to each other, presenting larger values of MFDI than the annual cycle for the historical period in all months of the year. In 2071-2100, there are virtually no changes relative to 2021-2050 for RCP2.6 but there is a large systematic positive change for RCP4.5 and an even larger change for RCP8.5.

Systematic changes in the annual cycles of simulation-based MFDI for the historical period and the future climate scenarios reflect changes in the annual cycles of temperature, relative humidity and precipitation. Figures 5.10, 5.11, 5.12 and 5.13 include these results for all RCPs and time periods considered.

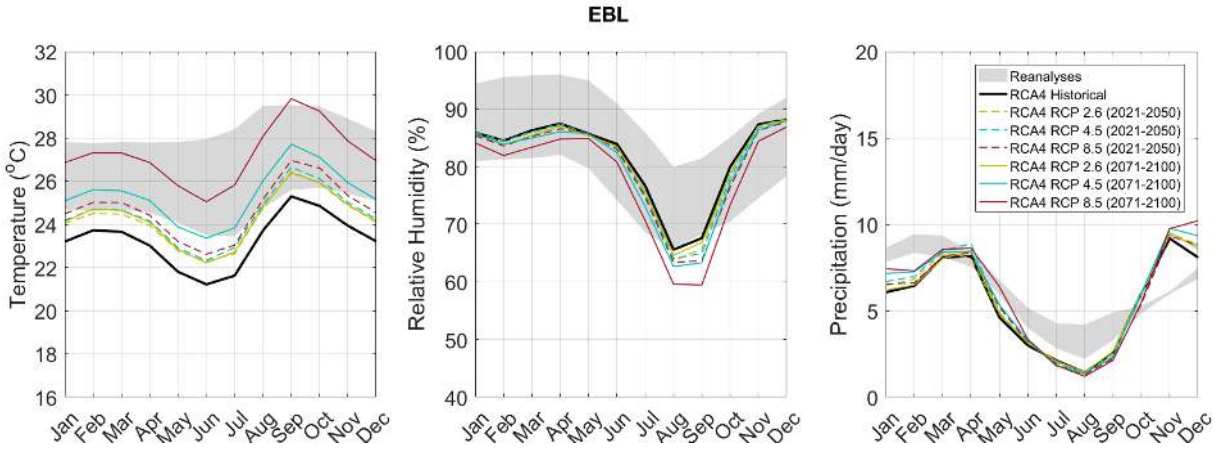

Figure 5.10: Annual cycles of simulated temperature (left panel), relative humidity (centre panel) and precipitation (right panel) for the *EBL* landcover as derived from RCM for the historical period (1976-2005) (solid black curve), for the mildest scenario (RCP2.6) (yellow curves), an intermediate scenario (RCP4.5) (blue curves) and the most severe scenario (RCP8.5) (red curves) for both future time periods considered: 2021-2050 (dashed) and 2071-2100 (solid). Grey area represents the observation-based data range from the three reanalyses, for reference.

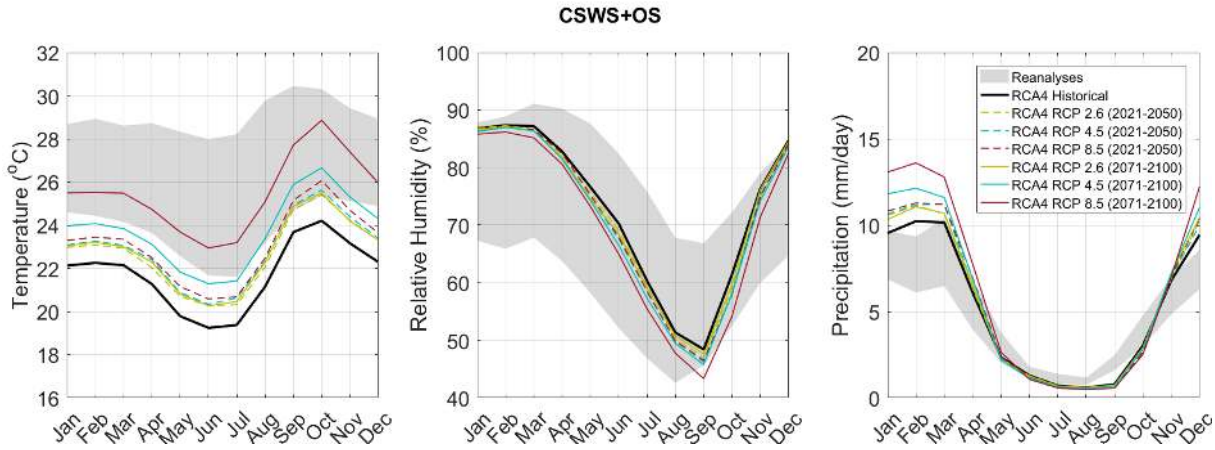

Figure 5.11: As in Figure 5.10 but regarding *CSWS+OS*.

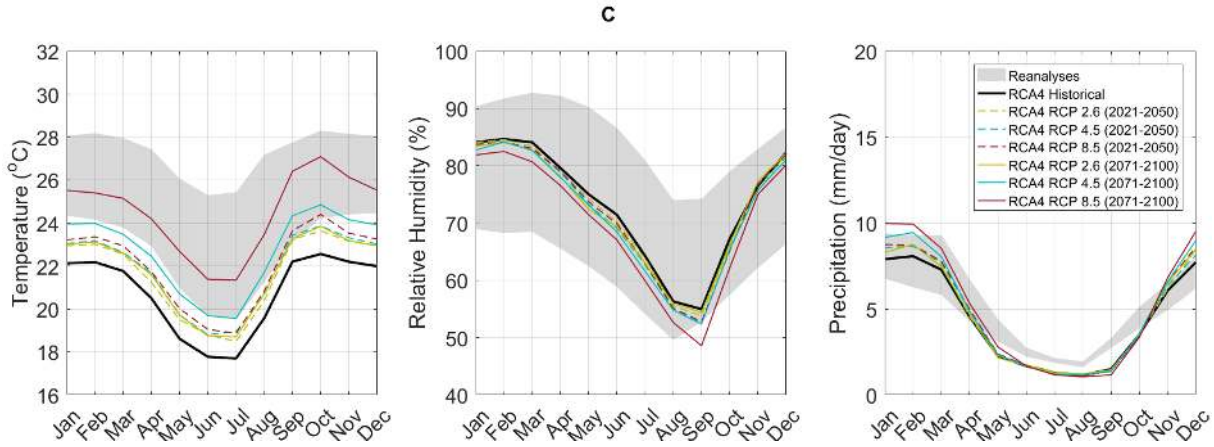

Figure 5.12: As in Figure 5.10 but regarding *C*.

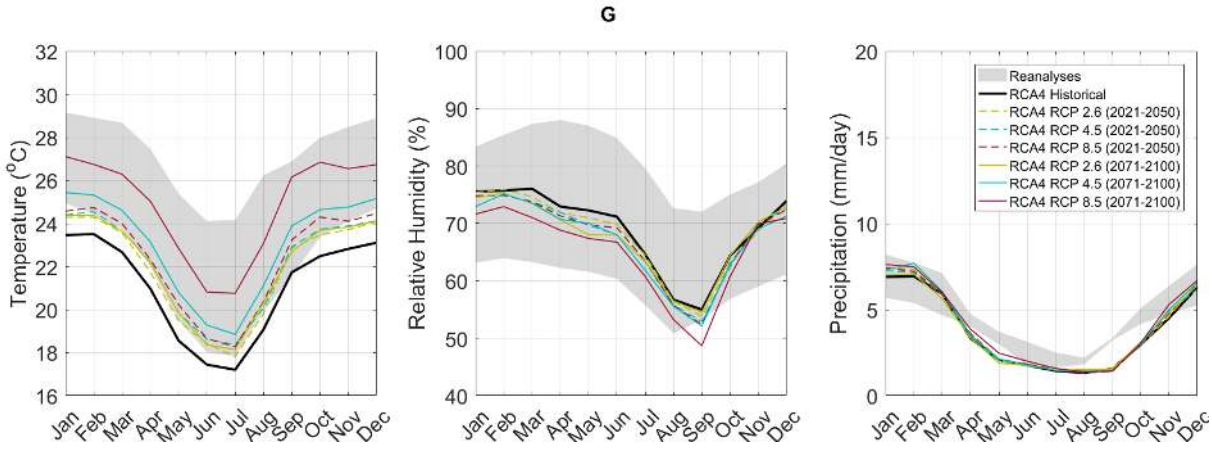

Figure 5.13: As in Figure 5.10 but regarding *G*.

There is a clear increase in T in all months for all vegetation types and scenarios, especially in 2071-2100 for RCP4.5 and RCP8.5. It's also worth noting that seasonal cycles of temperature for 2021-2050 are very similar across all scenarios.

On the other hand, for all vegetation types, the annual cycles of relative humidity present systematic decreases that are larger in August and September. All RCPs present similar RH annual cycles in each vegetation type that have systematically lower values of relative humidity than those of the historical period, and in 2071-2100 a large decrease relative to 2021-2050 is observed for RCP8.5.

Lastly, in the case of the annual cycle of precipitation, virtually no changes are observed from June to October in *EBL* and from May to October in the other vegetation types; changes in MFDI during the fire season for the historical period and the future scenarios are therefore determined by changes in temperature and relative humidity. In the case of *CSWS+OS* and to a lesser extent in *C*, there is an increase in the annual cycle of precipitation from December to March. The annual cycles of precipitation in 2021-2050 for all RCPs are very similar, however the curves for 2071-2100 show a marked increase, especially in RCP4.5 and RCP8.5. This is especially relevant because such strong changes in the precipitation cycle may alter the characteristics of vegetation cover and indirectly change the meteorological fire danger.

5.4 Future projections of burned area

The burned area models that were developed in previous sections were used to assess expected impacts on the burned area regime due to changes in simulation-based MFDI from the historical period to future climate scenarios.

Normal distributions were fitted to averages of $MFDI_{ERAI}$ over the fire season (i.e. over August, September and October) for *EBL*, and over September and October in *CSWS+OS*, *C* and *G*, for the 1981-2005 period. These are the same datasets used to develop the burned area models for each vegetation type in Section 5.2. Normal distributions were also fitted to $MFDI_{RCA4}$ using the same approach. Table 5.3 shows obtained estimates of mean and standard deviation for these datasets, and the results of testing the null hypothesis that data come from a normally distributed population with unknown mean and standard deviation using the Lilliefors test.

Table 5.3: Estimated mean and standard deviations of $MFDI_{ERAI}$ and MFDI as derived from the RCM ($MFDI_{RCA4}$) for the period 1981-2005, and p-values of Lilliefors test of normality for the main vegetation types.

Vegetation type	$MFDI_{ERAI}$			$MFDI_{RCA4}$		
	Mean	**St. Dev.**	**p-value**	**Mean**	**St. Dev.**	**p-value**
EBL (Aug-Sep-Oct)	0.09	0.03	0.2	0.24	0.03	0.2
CSWS+OS (Sep-Oct)	0.64	0.10	0.3	0.64	0.04	>0.5
C (Sep-Oct)	0.54	0.09	>0.5	0.56	0.04	>0.5
G (Sep-Oct)	0.57	0.08	0.4	0.60	0.03	>0.5

The null hypothesis of normality is accepted for samples of both observation-based and simulation-based MFDI at the 5% significance level in all vegetation types. There is however a strong contrast between results for *EBL* and the remaining vegetation types that is worth pointing out. In *EBL*, the values of $MFDI_{RCA4}$ are strongly biased towards large values, the mean value of 0.24 for simulation-based MFDI being much greater than $MFDI_{ERAI}$ that is only 0.09; however, both observation-based and simulation-based distributions present similar dispersion in turn of the mean, both with standard deviation of 0.03. In the other three vegetation types, the opposite is true; $MFDI_{RCA4}$ distributions have mean values very close to the corresponding distributions of $MFDI_{ERAI}$ but the RCM underestimates the variability in *CSWS+OS*, *C* and *G*, where the standard deviations are considerably smaller than those of the observation-based distributions.

Samples of simulation-based MFDI for each vegetation type are then corrected so that the fitted normal distributions have the same mean and standard deviation of the corresponding distributions of $MFDI_{ERAI}$. This is achieved using Equation 4.3, with μ_1 and σ_1 (μ_2 and σ_2) being replaced by the mean and the standard deviation of the simulation-based (ERA-I based) MFDI. Normal distributions were than fitted to simulation-based values of $MFDI_{RCA4}$ during the 30-year historical period (1976-2005) and during the two 30-year periods (2021-2050 and 2071-2100) of the three RCPs. The null hypothesis of normality is accepted at the 5% significance for all vegetation types, periods and scenarios, the exception being *C* in the case of RCP2.6 in 2071-2100 where the significance level is 2%.

All samples of $MFDI_{RCA4}$ were corrected using the corresponding transformation that was used to convert the simulation-based normal distribution into the observation-based one in 1981-2005. Samples of burned area for all vegetation types, scenarios and periods were then generated by applying the adequate burned area model to the appropriate corrected sample of observation-based MFDI ($MFDI_{RCA4-corr}$). Since the burned area model is linear and the distributions of $MFDI_{RCA4-corr}$ are normal, obtained samples of burned area also have normal distributions and may be characterized by their means and standard deviations.

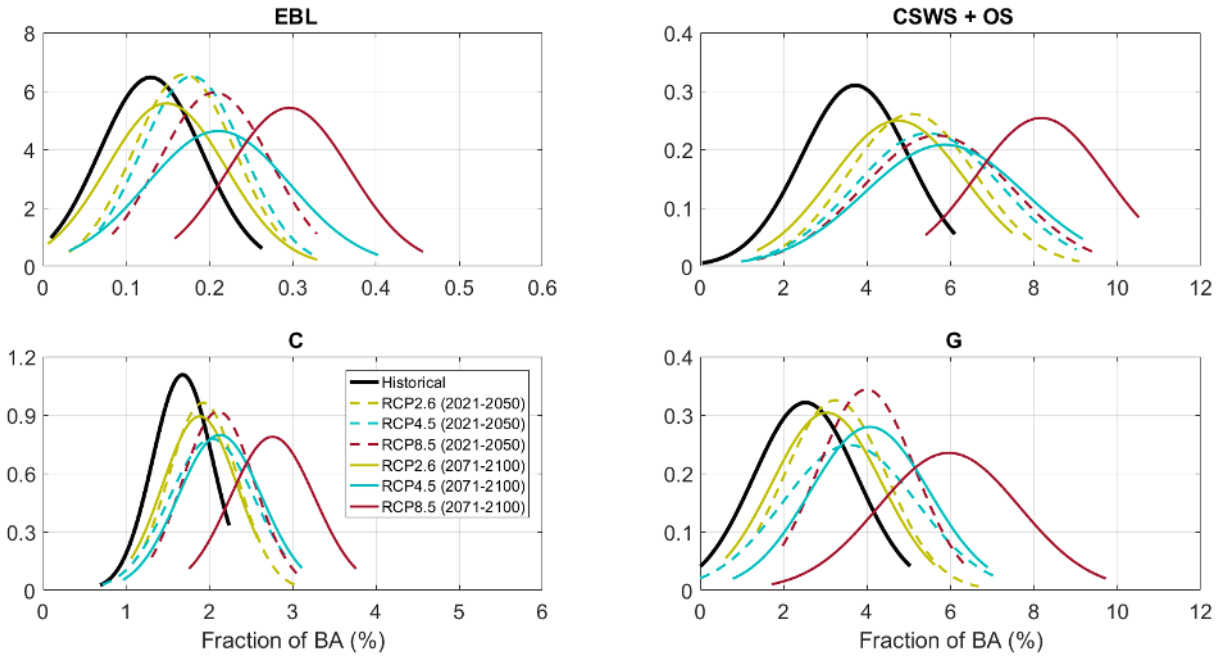

Figure 5.14: Normal distributions of burned area as estimated from the burned area models using simulation-based MFDI as predictor: for the historical period (1976-2005) (solid black curve); and for RCP2.6 (yellow curves), RCP4.5 (blue curves) and RCP8.5 (red curves) future climate scenarios for the periods 2021-2050 (dashed) and 2071-2100 (solid). The normal distributions were rescaled so that burned area is expressed in terms of fraction (%) of the total area occupied by each vegetation type.

Results obtained are shown in Figure 5.14 and it is worth noting that in order to compare changes in the distributions of different vegetation types, the normal distributions were rescaled, so that burned area is expressed in terms of fraction of the total area occupied by the corresponding vegetation type. Each vegetation type presents changes with characteristics of its own but in all cases future climate scenarios have larger means and standard deviations than the historical period, with RCP8.5 in 2071-2100 showing much higher bias and dispersion than the other scenarios. The case of *CSWS+OS* is especially conspicuous because it presents the largest increases in both mean and standard deviation of the fraction of BA. This is worth being emphasized, considering that *CSWS+OS* currently represents more than three fourths (76%) of the total burned area in Brazil.

As seen in Table 5.4, there is an overall agreement between biomes that in RCP2.6 2021-2050 the burned area will increase, only to decrease to a still higher than historical value in 2071-2100. This is consistent with this being the only scenario in which the radiative forcing decreases over the century, theoretically reaching 3.1 Wm^{-2} before it returns to 2.6 Wm^{-2} by 2100.

On the other hand, for all biomes, RCP4.5 and RCP8.5 results in 2071-2100 increase compared to their 2021-2050 counterparts. Increases for RCP4.5 in 2071-2100 are not as pronounced as those in the same period for RCP8.5, given the relatively ambitious emissions reductions in the former scenario as a result of stringent climate policies. RCP8.5 is consistent with high emissions and no reduction policy changes, resulting in much more pronounced average BA increase over the century. For both RCP4.5 and RCP8.5 and in both time periods, *C* is the biome with the least increase in average BA and the highest escalations are found in *G* and *EBL*.

Table 5.4: Differences in mean (standard deviation) of future BA from the historical period (1976-2005) for the main vegetation types.

Vegetation type	Differences in Mean (St. Dev) from the historical period (%)					
	RCP2.6		RCP4.5		RCP8.5	
	2021-2050	2071-2100	2021-2050	2071-2100	2021-2050	2071-2100
EBL	31	15	39	63	60	129
	(-2)	(16)	(-1)	(40)	(9)	(19)
CSWS+OS	37	27	47	56	53	120
	(19)	(24)	(36)	(49)	(38)	(22)
C	15	12	21	27	26	64
	(15)	(24)	(42)	(39)	(20)	(40)
G	29	20	42	61	58	137
	(-1)	(6)	(29)	(15)	(-7)	(37)

In the *CSWS+OS* biome, RCP4.5 and RCP8.5 achieve very similar mean BA values in 2021-2050: (15.2 ± 4.9) and $(15.8 \pm 5.0) \times 10\,000\ km^2$, respectively. This indicates a similar anthropogenic forcing in the first half of the century for both scenarios, but a distinct pathway from mid-century onwards. And although RCP2.6 corresponds to the most optimistic scenario with ambitious greenhouse gas emissions reductions, *CSWS+OS* BA average would still increase by a factor of 37% and 27% for the 2021-2050 and 2071-2100 period, respectively.

6. Final Remarks

This study is, to the best of the author's knowledge, the first validation of the MFDI fire danger index (known otherwise as *Risco de Fogo* in Setzer and Sismanoglu [2012]). Results show that MFDI can accurately replicate the inter and intra-annual variability of burned area for the main four Brazilian landcover types: *EBL*, *CSWS+OS*, *C* and *G*. It achieves high fire danger values in high burning months, and in *CSWS+OS* it further shows a delay from high fire danger to highest burned area, possibly due to *CSWS+OS* needing time to accumulate stress.

The methodology involved using simple linear regression models to estimate BA using MFDI as the predictor. All four models, for each vegetation type, were able to explain at least 50% of the inter-annual variability of burned area. *CSWS+OS* results are especially conspicuous, with 77% of the variability explained by the linear regression model, in agreement with its higher dependence to meteorological conditions. Results for *EBL*, on the other hand, with 51% of explained variability, suggest a weaker dependency on meteorological fire danger, consistent with this region being predominantly a humid biome (Amazon).

The RCA4 was overall capable of estimating present meteorological conditions as evaluated by the reanalyses. Relative humidity remained within the expected values, precipitation was slightly underestimated in the fire season months, and there is a noteworthy underestimation of temperature in all landcovers when compared to the three reanalyses. Nevertheless, simulated MFDI was able to follow the trends of observation-based fire danger keeping within the reanalyses range at most times; the only major difference being a significant overestimation of fire danger in *EBL* in the fire season months thanks to a pronounced decrease in precipitation estimated by the model in that period.

Future results show an overall agreement in increased fire danger and burned area for Brazil under all climate scenarios. In RCP4.5, the intermediate scenario, results indicate an expected increase of 39% in historical BA in *EBL* in the first half and reaching 60% by the end of the century, indicating that the Amazon rainforest might experience more wildfires than ever before, all other drivers remaining constant. Biomes such as Amazon are not structurally adapted to fire and may undergo progressive degradation under increasing fire danger. *CSWS+OS* and *G* also present very significant increases in BA, with at least a 40% increase in both periods. These vegetation types, contrary to the Amazon rainforest, are fire dependent which means that they may recover and adapt more easily to the increased fire danger (thus, possibility, fire activity) than fire-sensitive biomes. Nevertheless, high severity fires can still irreparably damage fire-prone ecosystems, particularly under the RCP8.5 scenario, where burned area is expected to double by the end of the century.

RCP8.5 shows similar trends to RCP4.5 but much more pronounced: for all biomes, the historical BA increases in at least 50% for the 2021-2050 period and, except in *C*, it doubles in 2071-2100 when compared to its historical value. On the other hand, RCP2.6 is the only scenario in which the average burned area is expected to decrease slightly on the second half of the century, based on changes in climate only. This scenario is the closest to the pledges made in the Paris Agreement to keep global warming bellow $1.5°C$ and, although it has been shown to be feasible still [Millar *et al.*, 2017], it requires quick and meaningful measures.

The expected changes in BA found here imply that, by the end of the century, the *CSWS+OS* vegetation type would burn regularly 16.3 thousand hectares per year under RCP4.5 or as much as a severe

year under RCP8.5 (22.7 thousand hectares a year), i.e. 6% and 8% of its total area on average per year. Moreover, the average burned area value from September to October for *CSWS+OS* by the end of the century in RCP8.5, would represent 83% of the highest total annual burned area ever recorded in Brazil (which was 27.5 thousand hectares in 2017; Figure 1.1). These results are of particular importance given that *CSWS+OS* represents a large part of most Brazilian biomes. They also shed light on the potential magnitude of changes in fire danger and burned area due to future changes in climate only. Results also illustrate that caution is needed when interpreting these curves: these scenarios do not take into account climate-vegetation feedbacks and thus assume that vegetation remains the same as it does in the current climate. This is likely not realistic, as biomes may not be able to cope with the changes in fire regime or climate conditions, and also because Brazil may likely have important changes in land-use practices. Although this is valid across all scenarios, this is especially true for RCP8.5 projections for 2071-2100, given that it assumes the biggest change in climatic parameters.

This discloses one limitation of this work: we assess the fire danger due to climatic changes, not considering anthropogenic factors and land cover change. Fire-climate-vegetation feedbacks are not incorporated into these calculations and can possibly alter the state of vegetation and have an increased warming effect on global climate through fire-related emissions. Nevertheless, climate-fire relationships should provide a general basis for understanding the natural seasonality and frequency of fire, given their correlation with meteorology and climatic events such as ENSO [Beckage *et al.*, 2005]. Furthermore, despite no evidence exists that the CO_2 fertilization effect has a marked role on rainforests on longer time scales, if this effect persists throughout the century, biome distribution does not change significantly according to several GCMs [Lapola *et al.*, 2009] in which case these projections could prove accurate. However, it is also possible that, if the CO_2 fertilization effect does not occur, there will be substantial shifts to drier and less productive biomes. Although this could possibly justify a static vegetation cover, future work includes adding a dynamic vegetation model to properly reproduce vegetation-climate interactions.

Even though fire activity is ultimately dependent on ignition, either natural or human, this is not taken into account here. Similarly, other components of fire regimes would need to be evaluated to provide a comprehensive view of fire conditions in Brazil: fire intensity for example, would have to be further analysed, given that it regards not only changes in the conditions for fire, but also the resources available to burn under those conditions [Krawchuk *et al.*, 2009]. Although, the MFDI described in Silva *et al.* [2016] does rate fire from Minimum to Critical, these metrics only regard how pre-disposed the vegetation is to burn, not the amount of vegetation available to burn. To that end, we would have to use a dynamic vegetation model as previously mentioned. Other noteworthy limitations need to be mentioned in order to correctly put into perspective the results and their applicability. Burned area data products derived from satellite also suffer from uncertainties, potentially missing some fires (smoldering fires in peatlands often evade detection) and may include non-vegetation fires. To overcome this shortcoming, the AQM product was used, which detects fires in Brazil otherwise not seen in satellite imagery. However, the number of fire pixels observed within a grid cell does not necessarily indicate the total area burned within the grid cell.

Also, these results are dependent on the RCA4 model configuration (as well as on the EC-Earth's). To evaluate model-dependent uncertainty, the analysis could be extended to an ensemble of different combinations of GCMs, RCMs and scenarios. Kloster and Lasslop [2017] have provided insights using ensemble forecasting fire occurrence, based on the the models from the CMIP5 experiment, and little consensus between models in present and future estimations. In the CMIP5 intercomparison, most land-surface models did not simulate fire, making it difficult to evaluate future fire patterns and feedbacks

with climate. However, a number of land-surface models already include prognostic fire modules, which allows capturing vegetation-climate interactions. Even though models suffer from several sources of uncertainty, projects such as the FireMIP [Rabin *et al.*, 2017] may contribute to better constrain model results and future estimates.

Finally, worth further emphasizing the role of human activity and policy on fire management. There are several aspects of fire that can be regulated and controlled, such as ignitions and fuel availability. Contrary to common belief, in some cases fire suppression is not a sustainable solution, as it produces unnaturally high fuel loadings that increase the risk of high-severity fires in forests characterized by frequent, low-severity fires [Turner, 2010]. Prescribed burning could provide a solution and play an important role in fire management, as it limits vegetation grown in certain seasons preventing future wildfires or lowering their severity. In light of a warmer future, forest management could also plant species that are adapted to the current and future climate instead of past climate in order to ensure that biomes could withstand changing fire regimes. The restoration and management of fire dependent ecosystems such as *cerrado* requires ecologically appropriate fire management that should be based on natural fire regimes, hence the importance of studies such as this.

References

Aldersley, A., Murray, S.J., and Cornell, S.E. (2011). Global and regional analysis of climate and human drivers of wildfire. *Science of The Total Environment*, 409(18), 3472 – 3481. ISSN 0048-9697. doi: https://doi.org/10.1016/j.scitotenv.2011.05.032.

Alduchov, O.A. and Eskridge, R.E. (1996). Improved Magnus Form Approximation of Saturation Vapor Pressure. *Journal of Applied Meteorology*, 35(4), 601–609. doi:10.1175/1520-0450(1996)035⟨0601:IMFAOS⟩2.0.CO;2.

Archibald, S., Lehmann, C.E.R., Gómez-Dans, J.L., and Bradstock, R.A. (2013). Defining pyromes and global syndromes of fire regimes. *Proceedings of the National Academy of Sciences*, 110(16), 6442–6447. ISSN 0027-8424. doi:10.1073/pnas.1211466110.

Baccini, A., *et al.* (2017). Tropical forests are a net carbon source based on aboveground measurements of gain and loss. *Science*, 358(6360), 230–234. ISSN 0036-8075. doi:10.1126/science.aam5962.

Beckage, B., Platt, W.J., and Panko, B. (2005). A Climate-Based Approach to the Restoration of Fire-Dependent Ecosystems. *Restoration Ecology*, 13(3), 429–431. ISSN 1526-100X. doi:10.1111/j.1526-100X.2005.00070.x.

Bond, W.J. and Keeley, J.E. (2005). Fire as a global 'herbivore': the ecology and evolution of flammable ecosystems. *Trends in Ecology & Evolution*, 20(7), 387–394. ISSN 0169-5347. doi:https://doi.org/10.1016/j.tree.2005.04.025.

Bosilovich, M.G., Chen, J., Robertson, F.R., and Adler, R.F. (2008). Evaluation of Global Precipitation in Reanalyses. *Journal of Applied Meteorology and Climatology*, 47(9), 2279–2299. doi:10.1175/2008JAMC1921.1.

Bowman, D.M.J.S., *et al.* (2009). Fire in the Earth System. *Science*, 324(5926), 481–484. ISSN 0036-8075. doi:10.1126/science.1163886.

Bradshaw, L.S., Deeming, J.E., Burgan, R.E., and Cohen, J.D. (1984). The 1978 National Fire-Danger Rating System: technical documentation. General Technical Report INT-169. Tech. rep., U.S. Department of Agriculture, Forest Service, Intermountain Forest and Range Experiment Station.

Brady, M.A., *et al.* (2007). *Developing a global early warning system for wildland fire*, chap. 20. Springer Berlin Heidelberg, Berlin, Heidelberg. ISBN 978-3-540-72746-0, pp. 355–366. doi:10.1007/978-3-540-72746-0_20.

Brando, P.M., *et al.* (2014). Abrupt increases in Amazonian tree mortality due to drought–fire interactions. *Proceedings of the National Academy of Sciences*, 111(17), 6347–6352. ISSN 0027-8424. doi:10.1073/pnas.1305499111.

Brown, P.T. and Caldeira, K. (2017). Greater future global warming inferred from Earths recent energy budget. *Nature*, 552, 45.

Brunke, M.A., Wang, Z., Zeng, X., Bosilovich, M., and Shie, C.L. (2011). An Assessment of the Uncertainties in Ocean Surface Turbulent Fluxes in 11 Reanalysis, Satellite-Derived, and Combined Global Datasets. *Journal of Climate*, 24(21), 5469–5493. doi:10.1175/2011JCLI4223.1.

Chen, Y., *et al.* (2011). Forecasting Fire Season Severity in South America Using Sea Surface Temperature Anomalies. *Science*, 334(6057), 787–791. ISSN 0036-8075. doi:10.1126/science.1209472.

Cochrane, M.A. and Schulze, M.D. (1999). Fire as a Recurrent Event in Tropical Forests of the Eastern Amazon: Effects on Forest Structure, Biomass, and Species Composition. *Biotropica*, 31(1), 2–16. ISSN 1744-7429.

Davidson, E.A., *et al.* (2012). The Amazon basin in transition. *Nature*, 481, 321.

Dee, D., Fasullo, J., Shea, D., Walsh, J., and National Center for Atmospheric Research Staff (Eds) (2016). Atmospheric Reanalysis: Overview & Comparison Tables. [online] UCAR NCAR The Climate Data Guide. Available at: `https://climatedataguide.ucar.edu/climate-data/atmospheric-reanalysis-overview-comparison-tables` [Accessed in 15 Jan. 2018].

Dee, D.P., *et al.* (2011). The ERA-Interim reanalysis: configuration and performance of the data assimilation system. *Quarterly Journal of the Royal Meteorological Society*, 137(656), 553–597. ISSN 1477-870X. doi:10.1002/qj.828.

Dieng, H.B., Cazenave, A., Meyssignac, B., von Schuckmann, K., and Palanisamy, H. (2017). Sea and land surface temperatures, ocean heat content, Earth's energy imbalance and net radiative forcing over the recent years. *International Journal of Climatology*, 37, 218–229. ISSN 1097-0088. doi:10.1002/joc.4996.

Dieterich, C., *et al.* (2013). Evaluation of the SMHI coupled atmosphere-ice-ocean model RCA4-NEMO. Tech. Rep. 47, Oceanography.

Dowdy, A.J., Mills, G.A., Finkele, K., and de Groot, W. (2010). Index sensitivity analysis applied to the Canadian Forest Fire Weather Index and the McArthur Forest Fire Danger Index. *Meteorological Applications*, 17(3), 298–312. ISSN 1469-8080. doi:10.1002/met.170.

Duffy, P.B., Brando, P., Asner, G.P., and Field, C.B. (2015). Projections of future meteorological drought and wet periods in the Amazon. *Proceedings of the National Academy of Sciences*, 112(43), 13172–13177. ISSN 0027-8424. doi:10.1073/pnas.1421010112.

Durigan, G. and Ratter, J.A. (2016). The need for a consistent fire policy for Cerrado conservation. *Journal of Applied Ecology*, 53(1), 11–15. ISSN 1365-2664. doi:10.1111/1365-2664.12559.

Dwyer, E., Pinnock, S., Gregoire, J.M., and Pereira, J.M.C. (2000). Global spatial and temporal distribution of vegetation fire as determined from satellite observations. *International Journal of Remote Sensing*, 21(6-7), 1289–1302. doi:10.1080/014311600210182.

ECMWF (n.d.). *Climate Reanalysis*. [online] European Centre for Medium-Range Weather Forecasts. Available at: `https://www.ecmwf.int/en/research/climate-reanalysis` [Accessed in 15 Jan. 2018].

Evans, J. (2011). CORDEX - An international climate downscaling initiative. In *19th International Congress on Modelling and Simulation, Perth, Australia*. pp. 12–16.

Filizola, N., *et al.* (2014). Was the 2009 flood the most hazardous or the largest ever recorded in the Amazon? *Geomorphology*, 215, 99–105. ISSN 0169-555X. doi:https://doi.org/10.1016/j.geomorph.2013.05.028.

Flannigan, M., *et al.* (2013). Global wildland fire season severity in the 21st century. *Forest Ecology and Management*, 294, 54 – 61. ISSN 0378-1127. doi:https://doi.org/10.1016/j.foreco.2012.10.022.

Friedl, M.A., *et al.* (2010). MODIS Collection 5 global land cover: Algorithm refinements and characterization of new datasets. *Remote Sensing of Environment*, 114(1), 168 – 182. ISSN 0034-4257. doi:https://doi.org/10.1016/j.rse.2009.08.016.

Geirinhas, J.L., Trigo, R.M., Libonati, R., Coelho, C.A.S., and Palmeira, A.C. (2017). Climatic and synoptic characterization of heat waves in Brazil. *International Journal of Climatology*, 38(4), 1760–1776. ISSN 1097-0088. doi:10.1002/joc.5294.

Gelaro, R., *et al.* (2017). The Modern-Era Retrospective Analysis for Research and Applications, Version 2 (MERRA-2). *Journal of Climate*, 30(14), 5419–5454. doi:10.1175/JCLI-D-16-0758.1.

Giglio, L., Boschetti, L., Roy, D., Hoffmann, A.A., and Humber, M. (2016). Collection 6 MODIS Burned Area Product Users Guide Version 1.0. Tech. rep., MODIS FIRE.

Giglio, L., Csiszar, I., and Justice, C.O. (2006). Global distribution and seasonality of active fires as observed with the Terra and Aqua Moderate Resolution Imaging Spectroradiometer (MODIS) sensors. *Journal of Geophysical Research: Biogeosciences*, 111(G2), n/a–n/a. ISSN 2156-2202. doi:10.1029/2005JG000142. G02016.

Giglio, L., Loboda, T., Roy, D.P., Quayle, B., and Justice, C.O. (2009). An active-fire based burned area mapping algorithm for the MODIS sensor. *Remote Sensing of Environment*, 113(2), 408 – 420. ISSN 0034-4257. doi:https://doi.org/10.1016/j.rse.2008.10.006.

Giglio, L., Randerson, J.T., and van der Werf, G.R. (2013). Analysis of daily, monthly, and annual burned area using the fourth-generation global fire emissions database (GFED4). *Journal of Geophysical Research: Biogeosciences*, 118(1), 317–328. ISSN 2169-8961. doi:10.1002/jgrg.20042.

Gillett, N.P., Weaver, A.J., Zwiers, F.W., and Flannigan, M.D. (2004). Detecting the effect of climate change on Canadian forest fires. *Geophysical Research Letters*, 31(18), n/a–n/a. ISSN 1944-8007. doi:10.1029/2004GL020876. L18211.

Giorgi, F. (2006). Regional climate modeling: Status and perspectives. *J. Phys. IV France*, 139, 101–118. doi:10.1051/jp4:2006139008.

Giorgi, F., Jones, C., and Asrar, G.R. (2009). Addressing climate information needs at the regional level: the CORDEX framework. *Bulletin - World Meteorological Organization*, 58(3), 175–183.

Guimberteau, M., *et al.* (2013). Future changes in precipitation and impacts on extreme streamflow over Amazonian sub-basins. *Environmental Research Letters*, 8(1), 014035.

Gutowski, J., *et al.* (2016). WCRP COordinated Regional Downscaling EXperiment (CORDEX): A diagnostic MIP for CMIP6. *Geoscientific Model Development*, 9(11), 4087–4095. ISSN 1991-959X. doi:10.5194/gmd-9-4087-2016.

Hantson, S., Pueyo, S., and Chuvieco, E. (2015). Global fire size distribution is driven by human impact and climate. *Global Ecology and Biogeography*, 24(1), 77–86. ISSN 1466-8238. doi:10.1111/geb.12246.

Hardesty, J., Myers, R., and Fulks, W. (2005). Fire, Ecosystems, and People: A Preliminary Assessment of Fire as a Global Conservation Issue. *The George Wright Forum*, 22(4), 78–87. ISSN 07324715.

Hardy, C.C. (2005). Wildland fire hazard and risk: Problems, definitions, and context. *Forest Ecology and Management*, 211(1), 73 – 82. ISSN 0378-1127. doi:https://doi.org/10.1016/j.foreco.2005.01.029.

Hastie, T., Tibshirani, R., and Friedman, J. (2009). *The Elements of Statistical Learning: Data Mining, Inference, and Prediction*. Springer-Verlag, 2 ed.

Haustein, K., *et al.* (2017). A real-time Global Warming Index. *Scientific Reports*, 7(1), 15417. ISSN 2045-2322.

Hazeleger, W., *et al.* (2012). EC-Earth V2.2: description and validation of a new seamless earth system prediction model. *Climate Dynamics*, 39(11), 2611–2629. ISSN 1432-0894. doi:10.1007/s00382-011-1228-5.

Hoffmann, W.A., *et al.* (2012). Fuels or microclimate? Understanding the drivers of fire feedbacks at savannaforest boundaries. *Austral Ecology*, 37(6), 634–643. ISSN 1442-9993. doi:10.1111/j.1442-9993.2011.02324.x.

INPE (2017). *Monitoramento dos Focos Ativos por Países*. [online] Instituto Nacional de Pesquisas Espaciais. Available at: `http://www.inpe.br/queimadas/portal/estatistica_paises` [Accessed in 15 Jan. 2018].

IPCC (2013). *Climate Change 2013: The Physical Science Basis. Contribution of Working Group I to the Fifth Assessment Report of the Intergovernmental Panel on Climate Change*. 1535 pp., Cambridge University Press, Cambridge, United Kingdom and New York, NY, USA. ISBN ISBN 978-1-107-66182-0. doi:10.1017/CBO9781107415324.

Iqbal, W., *et al.* (2017). Mean climate and representation of jet streams in the CORDEX South Asia simulations by the regional climate model RCA4. *Theoretical and Applied Climatology*, 129(1), 1–19. ISSN 1434-4483. doi:10.1007/s00704-016-1755-4.

JPL (n.d.). *CORDEX - Introduction*. [online] Jet Propulsion Laboratory. Available at: `https://rcmes.jpl.nasa.gov/content/cordex` [Accessed in 15 Jan. 2018].

Kanamitsu, M., *et al.* (2002). NCEP-DOE AMIP-II Reanalysis (R-2). *Bulletin of the American Meteorological Society*, 83(11), 1631–1643. doi:10.1175/BAMS-83-11-1631.

Keetch, J.J. and Byram, G.M. (1968). A Drought Index for Forest Fire Control. Res. Pap. SE-38. Asheville, NC: U.S. Department of Agriculture, Forest Service, Southeastern Forest.

Kleschenko, A., Grom, L., Ndiaye, M., and Stefanski, R. (2004). The impacts of agrometeorological applications for sustainable management of farming, forestry and livestock systems. Tech. rep., CAgM report.

Kloster, S. and Lasslop, G. (2017). Historical and future fire occurrence (1850 to 2100) simulated in CMIP5 Earth System Models. *Global and Planetary Change*, 150, 58 – 69. ISSN 0921-8181. doi: https://doi.org/10.1016/j.gloplacha.2016.12.017.

Koenigk, T., *et al.* (2013). Arctic climate change in 21st century CMIP5 simulations with EC-Earth. *Climate Dynamics*, 40(11), 2719–2743. ISSN 1432-0894. doi:10.1007/s00382-012-1505-y.

Krawchuk, M.A., Moritz, M.A., Parisien, M.A., Van Dorn, J., and Hayhoe, K. (2009). Global Pyrogeography: the Current and Future Distribution of Wildfire. *PLOS ONE*, 4(4), 1–12. doi: 10.1371/journal.pone.0005102.

Lapola, D.M., Oyama, M.D., and Nobre, C.A. (2009). Exploring the range of climate biome projections for tropical South America: The role of CO_2 fertilization and seasonality. *Global Biogeochemical Cycles*, 23(3), n/a–n/a. ISSN 1944-9224. doi:10.1029/2008GB003357.

Lawrence, M.G. (2005). The Relationship between Relative Humidity and the Dewpoint Temperature in Moist Air: A Simple Conversion and Applications. *Bulletin of the American Meteorological Society*, 86(2), 225–233. doi:10.1175/BAMS-86-2-225.

Le Page, Y., *et al.* (2017). Synergy between land use and climate change increases future fire risk in Amazon forests. *Earth System Dynamics*, 8(4), 1237–1246. doi:10.5194/esd-8-1237-2017.

Le Quéré, C., *et al.* (2017). Global carbon budget 2017. *Earth System Science Data Discussions*, 1–79. ISSN 1866-3591. doi:10.5194/essd-2017-123.

Li, Z., Nadon, S., and Cihlar, J. (2000). Satellite-based detection of Canadian boreal forest fires: Development and application of the algorithm. *International Journal of Remote Sensing*, 21(16), 3057–3069. doi:10.1080/01431160050144956.

Libonati, R., DaCamara, C.C., Pereira, J.M.C., and Peres, L.F. (2011). On a new coordinate system for improved discrimination of vegetation and burned areas using MIR/NIR information. *Remote Sensing of Environment*, 115(6), 1464 – 1477. ISSN 0034-4257. doi:https://doi.org/10.1016/j.rse.2011.02.006.

Libonati, R., DaCamara, C.C., Setzer, A.W., Morelli, F., and Melchiori, A.E. (2015). An Algorithm for Burned Area Detection in the Brazilian Cerrado Using 4 μm MODIS Imagery. *Remote Sensing*, 7(11), 15782–15803. ISSN 2072-4292. doi:10.3390/rs71115782.

Lilliefors, H.W. (1967). On the Kolmogorov-Smirnov Test for Normality with Mean and Variance Unknown. *Journal of the American Statistical Association*, 62(318), 399–402. doi:10.1080/01621459.1967.10482916.

Liu, Y., Stanturf, J., and Goodrick, S. (2010). Trends in global wildfire potential in a changing climate. *Forest Ecology and Management*, 259(4), 685 – 697. ISSN 0378-1127. doi:https://doi.org/10.1016/j.foreco.2009.09.002.

Maestrini, B., Alvey, E.C., Hurteau, M.D., Safford, H., and Miesel, J.R. (2017). Fire severity alters the distribution of pyrogenic carbon stocks across ecosystem pools in a Californian mixed-conifer forest. *Journal of Geophysical Research: Biogeosciences*, 122(9), 2338–2355. ISSN 2169-8961. doi:10.1002/2017JG003832.

Malhi, Y., *et al.* (2009). Exploring the likelihood and mechanism of a climate-change-induced dieback of the Amazon rainforest. *Proceedings of the National Academy of Sciences*, 106(49), 20610–20615. ISSN 0027-8424. doi:10.1073/pnas.0804619106.

Marengo, J.A., Tomasella, J., Alves, L.M., Soares, W.R., and Rodriguez, D.A. (2011). The drought of 2010 in the context of historical droughts in the Amazon region. *Geophysical Research Letters*, 38(12), n/a–n/a. ISSN 1944-8007. doi:10.1029/2011GL047436.

Marengo, J.A., *et al.* (2012). Development of regional future climate change scenarios in South America using the Eta CPTEC/HadCM3 climate change projections: climatology and regional analyses for the Amazon, São Francisco and the Paraná River basins. *Climate Dynamics*, 38(9), 1829–1848. ISSN 1432-0894. doi:10.1007/s00382-011-1155-5.

McArthur, A.G. (1967). *Fire behaviour in eucalypt forests*. Forestry and Timber Bureau.

Millar, R.J., *et al.* (2017). Emission budgets and pathways consistent with limiting warming to 1.5°C. *Nature Geoscience*, 10, 741.

Mölders, N. (2010). Comparison of Canadian Forest Fire Danger Rating System and National Fire Danger Rating System fire indices derived from Weather Research and Forecasting (WRF) model data for the June 2005 Interior Alaska wildfires. *Atmospheric Research*, 95(2), 290 – 306. ISSN 0169-8095. doi:https://doi.org/10.1016/j.atmosres.2009.03.010.

Moriondo, M., *et al.* (2006). Potential impact of climate change on fire risk in the Mediterranean area. *Climate Research*, 31(1), 85–95. ISSN 0936577X, 16161572.

Moritz, M., Krawchuk, M., and Parisien, M. (2010). Pyrogeography: Understanding the ecological niche of fires. *PAGES Newsletter*, 18(2), 83–85.

Moritz, M.A., *et al.* (2012). Climate change and disruptions to global fire activity. *Ecosphere*, 3(6), 1–22. ISSN 2150-8925. doi:10.1890/ES11-00345.1.

Mutch, R.W. (1970). Wildland Fires and Ecosystems - A Hypothesis. *Ecology*, 51(6), 1046–1051. ISSN 1939-9170. doi:10.2307/1933631.

Myers, N., Mittermeier, R.A., Mittermeier, C.G., da Fonseca, G.A.B., and Kent, J. (2000). Biodiversity hotspots for conservation priorities. *Nature*, 403, 853.

Nature Climate Change (2017). Spreading like wildfire [editorial]. Nature Climate Change, 7, 755.

Nigam, S. and Ruiz-Barradas, A. (2006). Seasonal Hydroclimate Variability over North America in Global and Regional Reanalyses and AMIP Simulations: Varied Representation. *Journal of Climate*, 19(5), 815–837. doi:10.1175/JCLI3635.1.

NOAA (2017). *Extremely active 2017 Atlantic hurricane season finally ends*. [online] National Oceanic and Atmospheric Administration. Available at: `http://www.noaa.gov/media-release/extremely-active-2017-atlantic-hurricane-season-finally-ends` [Accessed in 15 Jan. 2018].

Oliver, J.E. (2005). *Encyclopedia of World Climatology*. Springer.

Page, S.E., *et al.* (2002). The amount of carbon released from peat and forest fires in Indonesia during 1997. *Nature*, 420, 61.

Panisset, J.S., *et al.* (2018). Contrasting patterns of the extreme drought episodes of 2005, 2010 and 2015 in the Amazon Basin. *International Journal of Climatology*, 38(2), 1096–1104. ISSN 1097-0088. doi: 10.1002/joc.5224.

Pausas, J.G. and Ribeiro, E. (2013). The global fire-productivity relationship. *Global Ecology and Biogeography*, 22(6), 728–736. ISSN 1466-8238. doi:10.1111/geb.12043.

Pereira, M.G., Calado, T.J., DaCamara, C.C., and Calheiros, T. (2013). Effects of regional climate change on rural fires in Portugal. *Clim Res*, 57(3), 187–200.

Perkins, S.E., Alexander, L.V., and Nairn, J.R. (2012). Increasing frequency, intensity and duration of observed global heatwaves and warm spells. *Geophysical Research Letters*, 39(20). ISSN 1944-8007. doi:10.1029/2012GL053361.

Prentice, I.C., *et al.* (2011). Modeling fire and the terrestrial carbon balance. *Global Biogeochemical Cycles*, 25(3). ISSN 1944-9224. doi:10.1029/2010GB003906.

Programa Queimadas INPE (2013). *Queimadas CPTEC/INPE Documentos*. [online] INPE. Available at: `http://queimadas.cptec.inpe.br/~rqueimadas/documentos/` [Accessed in 15 Jan. 2018].

Rabin, S.S., *et al.* (2017). The Fire Modeling Intercomparison Project (FireMIP), phase 1: experimental and analytical protocols with detailed model descriptions. *Geoscientific Model Development*, 10(3), 1175–1197. doi:10.5194/gmd-10-1175-2017.

Russo, S., *et al.* (2014). Magnitude of extreme heat waves in present climate and their projection in a warming world. *Journal of Geophysical Research: Atmospheres*, 119(22), 12,500–12,512. ISSN 2169-8996. doi:10.1002/2014JD022098.

Rusticucci, M. (2012). Observed and simulated variability of extreme temperature events over South America. *Atmospheric Research*, 106, 1 – 17. ISSN 0169-8095. doi:https://doi.org/10.1016/j.atmosres.2011.11.001.

Samuelsson, P., Gollvik, S., Kupiainen, M., Kourzeneva, E., and van de Berg, W.J. (2015). The surface processes of the Rossby Centre regional atmospheric climate model (RCA4). Tech. Rep. 157, Climate research - Rossby Centre.

Samuelsson, P., *et al.* (2011). The Rossby Centre Regional Climate model RCA3: model description and performance. *Tellus A*, 63(1), 4–23. ISSN 1600-0870. doi:10.1111/j.1600-0870.2010.00478.x.

Schimel, D. and Baker, D. (2002). The wildfire factor. *Nature*, 420, 29.

Setzer, A.W. and Sismanoglu, R.A. (2012). Risco de Fogo: Metodologia do Cálculo - Descrição sucinta da Versão 9. Tech. rep., Instituto Nacional de Pesquisas Espaciais - INPE.

Setzer, A.W., Sismanoglu, R.A., and Martins, G. (2017). Metodologia do Cálculo do Risco de Fogo do Programa Queimadas do INPE - Versão 10. Tech. rep., Instituto Nacional de Pesquisas Espaciais - INPE.

Shlisky, A., Meyer, R., Waugh, J., and Blankenship, K. (2008). Fire, nature, and humans: global challenges for conservation. *Fire Management Today*, 68(4), 36–42.

Silva, P., Bastos, A., DaCamara, C.C., and Libonati, R. (2016). Future Projections of Fire Occurrence in Brazil Using EC-Earth Climate Model. *Revista Brasileira de Meteorologia*, 31, 288 – 297. ISSN 0102-7786. doi:http://dx.doi.org/10.1590/0102-778631320150142.

Staver, A.C., Archibald, S., and Levin, S.A. (2011). The Global Extent and Determinants of Savanna and Forest as Alternative Biome States. *Science*, 334(6053), 230–232. ISSN 0036-8075. doi:10.1126/science.1210465.

Sterl, A., *et al.* (2012). A look at the ocean in the EC-Earth climate model. *Climate Dynamics*, 39(11), 2631–2657. ISSN 1432-0894. doi:10.1007/s00382-011-1239-2.

Stevens-Rumann, C.S., *et al.* (2018). Evidence for declining forest resilience to wildfires under climate change. *Ecology Letters*, 21(2), 243–252. ISSN 1461-0248. doi:10.1111/ele.12889.

Strahler, A., *et al.* (1996). MODIS BRDF/Albedo Product: Algorithm Theoretical Basis Document Version 4.0. Tech. rep., U.S. Geological Survey.

Strandberg, G., *et al.* (2015). CORDEX scenarios for Europe from the Rossby Centre regional climate model RCA4. Tech. Rep. 116, Climate research - Rossby Centre.

Strassburg, B.B.N., *et al.* (2017). Moment of truth for the Cerrado hotspot. *Nature Ecology &Amp; Evolution*, 1, 0099.

Thonicke, K., *et al.* (2010). The influence of vegetation, fire spread and fire behaviour on biomass burning and trace gas emissions: results from a process-based model. *Biogeosciences*, 7(6), 1991–2011. doi:10.5194/bg-7-1991-2010.

Trenberth, K.E., Fasullo, J.T., and Balmaseda, M.A. (2014). Earth's Energy Imbalance. *Journal of Climate*, 27(9), 3129–3144. doi:10.1175/JCLI-D-13-00294.1.

Trenberth, K.E., Fasullo, J.T., and Mackaro, J. (2011). Atmospheric Moisture Transports from Ocean to Land and Global Energy Flows in Reanalyses. *Journal of Climate*, 24(18), 4907–4924. doi:10.1175/2011JCLI4171.1.

Turner, M.G. (2010). Disturbance and landscape dynamics in a changing world. *Ecology*, 91(10), 2833–2849. ISSN 1939-9170. doi:10.1890/10-0097.1.

Turner, M.G., Hargrove, W.W., Gardner, R.H., and Romme, W.H. (1994). Effects of fire on landscape heterogeneity in Yellowstone National Park, Wyoming. *Journal of Vegetation Science*, 5(5), 731–742. ISSN 1654-1103. doi:10.2307/3235886.

UNFCCC (2017). Paris agreement. Paris: United Nations Framework Convention on Climate Change. Pp.1-27.

USGS (2017). *Burned Area Essential Climate Variable (BAECV)*. [online] U.S. Geological Survey. Available at: `https://remotesensing.usgs.gov/ecv/BA_overview.php` [Accessed in 15 Jan. 2018].

van der Werf, G.R., *et al.* (2004). Continental-Scale Partitioning of Fire Emissions During the 1997 to 2001 El Niño/La Niña Period. *Science*, 303(5654), 73–76. ISSN 0036-8075. doi:10.1126/science.1090753.

van der Werf, G.R., *et al.* (2017). Global fire emissions estimates during 1997-2016. *Earth System Science Data*, 9(2), 697–720. doi:10.5194/essd-9-697-2017.

van Vuuren, D.P., *et al.* (2011). The representative concentration pathways: an overview. *Climatic Change*, 109(1), 5. ISSN 1573-1480. doi:10.1007/s10584-011-0148-z.

Voiland, A. (2017). *Severe Monsoon Rains Flood South Asia*. [online] NASA Earth Observatory. Available at: `https://earthobservatory.nasa.gov/IOTD/view.php?id=90920` [Accessed in 15 Jan. 2018].

von Schuckmann, K., *et al.* (2016). An imperative to monitor Earth's energy imbalance. *Nature Climate Change*, 6. doi:http://dx.doi.org/10.1038/nclimate2876.

Wagner, C.E.V. (1987). Development and structure of the canadian forest fire weather index system. *Can. For. Serv., Forestry Tech. Rep*.

Westerling, A.L., Hidalgo, H.G., Cayan, D.R., and Swetnam, T.W. (2006). Warming and Earlier Spring Increase Western U.S. Forest Wildfire Activity. *Science*, 313(5789), 940–943. ISSN 0036-8075. doi:10.1126/science.1128834.

Wilks, D. (1995). *Statistical Methods in the Atmospheric Sciences*, vol. 10. Academic Press, 3 ed.

Williams, F. (1977). Mechanisms of fire spread. *Symposium (International) on Combustion*, 16(1), 1281 – 1294. ISSN 0082-0784. doi:https://doi.org/10.1016/S0082-0784(77)80415-3.

Wuyts, B., Champneys, A.R., and House, J.I. (2017). Amazonian forest-savanna bistability and human impact. *Nature Communications*, 8, 15519.